CHAPTER 1

INTRODUCTION

Proton conducting polymer electrolytes with a variety of properties has been the focus of polymer research for many years due to possibility of their application in various electrochemical devices, e.g., fuel cells and electrochromic devices. Since their development in the 1960s, perfluorinated ionomers have emerged as standard materials for low-temperature fuel cell applications because of their high proton conductivity and their excellent chemical and thermal stability.

In addition to these factors, which decrease the total efficiency of the system, the high price, as well as difficult recycling or disposal of the perfluorinated materials, has slowed wide-spread and economical application. Accordingly, a variety of alternative approaches using materials that are cheaper and/or more suitable for higher temperatures have been explored, among which are non-fluorinated ionomers and composite membranes.

The focus on polymeric materials in which proton conduction does not depend on the presence of an aqueous phase. In general, there are two fundamental approaches toward such membranes. The first one is simply based on the substitution of the water with another suitable proton solvent that is capable of conducting protons in a similar way at higher temperatures. A second approach points toward fully polymeric systems that exhibit proton conductivity as an intrinsic property. In principle, these materials consist of an acid-doped proton acceptor (or vice versa) that forms mobile protonic defects (excess protons or proton vacancies, respectively) (Schuster et al., 2003).

There is an increasing interest in anhydrous proton conducting polymer electrolytes due to their use as membranes in fuel cells at intermediate temperatures ($T>100\ ^{o}C$) (Schuster et al., 2003, Smitha et al., 2005, Kreuer et al., 2001). During last few decades, polymer-acid

complexes have been considered as an alternative route for anhydrous proton conductors that can maintain high conductivity at medium temperatures (Smitha et al., 2005). In these systems, polymers bearing basic sites interact with the strong acid via hydrogen bonds and proton conduction occurs through structure diffusion, i.e., jump reorientation mechanism between Bronsted acid base pairs (Schuster et al., 2003). Although these host-guest systems illustrate high proton conductivity, high acid containing materials sacrifice chemical and mechanical stability especially at higher temperatures (Schuster et al., 2003, Jannasch, 2003, Bozkurt et al., 2001, Meyer et al., 2001). Among these family of materials, H_3PO_4-doped polybenzimidazole (PBI) received much attention and seems to be more promising in terms of its thermal and chemical stability (Schechter et al., 2002).

Anhydrous neutral or basic proton conducting materials are also under-development with particular interest in heterocyclic compounds. Recent attempt was the preparation of hybrid electrolytes by incorporation of imidazole or benzimidazole either in ionic liquids (Sun et al., 2001) or in polymer matrix (Bozkurt et al., 2003, Erdemi et al., 2004, Sevil et al., 2004, Yamada et al., 2004). The proton conduction may occur through non-vehicular mechanism where proton transferred from site to site by hydrogen bond breaking and forming processes (Kreuer et al., 1998).

CHAPTER 2

PROTON CONDUCTION

Proton transfer mechanisms are well-established phenomena in nature. Most biochemical reactions are very sensitive to changes in the pH of the surrounding enviroment so proton transfer serves as a vital route in the cell pH stabilization. In biological systems, while information is generally transferred via metal ions, all processes which convert energy from one form to another involve protonation and deprotonation reactions.

Proton conductivity also plays a key role in other important processes as diverse as the photosynthesis in plants to the generation of clean electrical energy in fuel cell power plants. Such as extensive range of proton transport and transfer phenomena has therefore attracted interest from material through understanding of the mechanisms and procosses has been established. Hence, the identification and development of new proton conducting materials, especially for the solid electrolyte domain, relies heavily on this collective knowledge.

2.1 PROTON CONDUCTION MECHANISMS

The proton is unique in that it is the only ion which possesses no electronic shell . It therefore strongly interacts with the electron density of its environment. In the case of metals, the proton interacts with the electron density of the conduction band, and is considered to be a hydrogen atom with a protonic or hydridic character. Metals are also unique in that they allow the proton(hydrogen) to have a high coordination number, typically four or six at a tetrahedral or octahedral site (Kreuer, 1988). In non-metallic compounds, the proton interacts strongly with the electron density of only one or two

nearest neighbours. If this is a single oxygen atom, while being well separated from other electronegative species, this results in the formation of an O-H bond which is less than 100 pm in length (Figure 2.1a), compared to ~140 pm for the ionic radius of the oxide ion. In this state, the protons equilibrium position lies deeply embedded in the electron density of the oxygen. For medium distances between two oxygen atoms (~250-280 pm), the proton may be involved in two bonds: a short, strong bond with a proton donor and a long, weak bond with a proton acceptor. This is the case of an asymmetrical hydrogen bond (O-H…O) which is directional in character (Figure 2.1b). For shorter oxygen separations (~240 pm), a symmetrical hydrogen bond may be formed where the proton is involved in two equivalent bonds (Schuster et al., 1976) (Figure 2.1c).

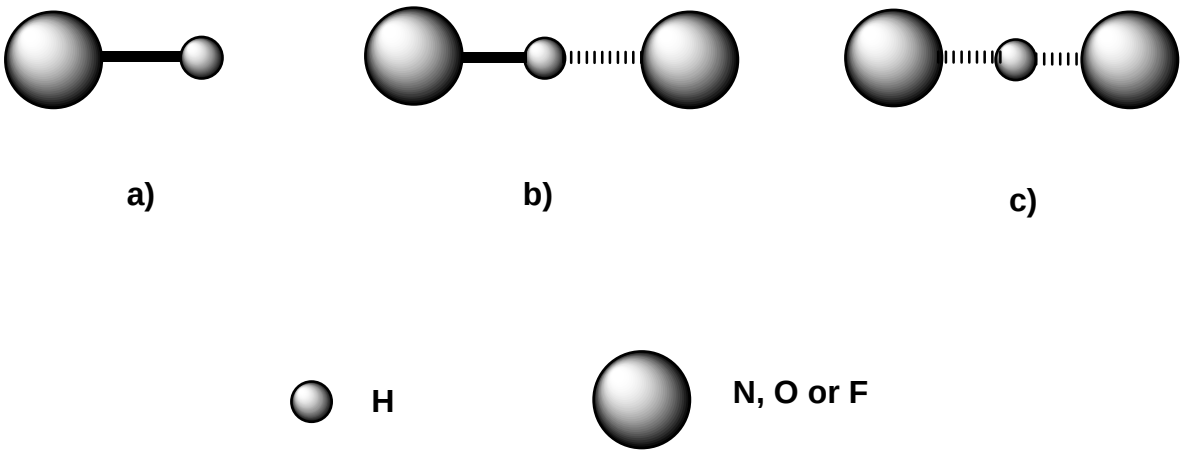

Figure 2.1 Schematic representation showing different classes of proton interaction in a nonmetallic environment with one or two basic entities (Schuster et al., 1976).

Proton transfer phenomena follow two principal mechanisms where the proton remains shielded by electron density along its entire diffusion path, so that in effect the momentary existence of a free proton is not seen. The most trivial case of proton migration requires the translational dynamics of bigger species: this is the **vehicle mechanism** (Kreuer et al., 1982). In this mechanism the proton diffuses through the medium together with a "vehicle" (for example, with H_2O as H_3O^+). The counter diffusion of unprotonated vehicles (H_2O) allows the net transport of protons. The observed conductivity, therefore, is directly dependant on the rate of vehicle diffusion (Figure 2.2). In the other principal mechanism, the vehicles show pronounced local

dynamics but reside on their sites. The protons are transferred from one vehicle to the other by hydrogen bonds (proton hopping). Simultaneous reorganization of the proton environment, consisting of reorientation of individual species or even more extended ensembles, then leads in the formation of an uninterrupted path for proton migration. This mechanism is known as the **Grotthuss mechanism**. This reorganization usually involves the reorientation of solvent dipoles (for example H_2O), which is an inherent part of establishing the proton diffusion pathway. The rates of proton transfer and reorganization of its environment affect directly this mechanism. All rates directly connected to the diffusion of protons are schematically illustrated in Figure 2.2.

A) Grotthuss mechanism

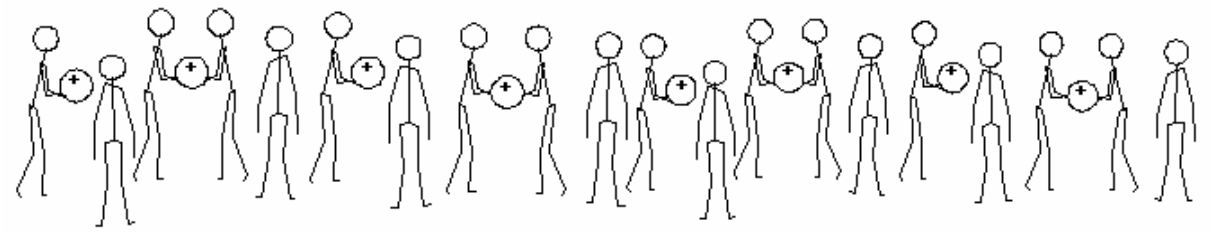

B) Vehicle mechanism

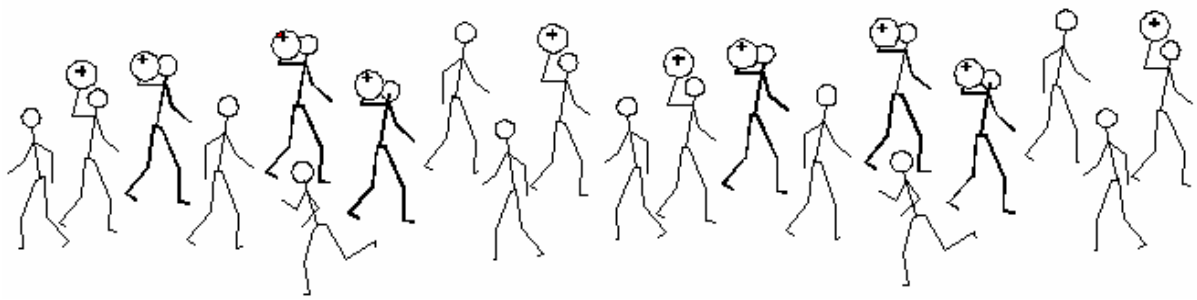

Figure 2.2 Schematic representation of phenomena involved in proton conduction mechanisms (Kreuer et al., 1982).

These two principle mechanisms essentially reflect the difference in nature of the hydrogen bonds formed between the protonated species and their environment. In media which supports strong hydrogen bonding, the Grotthuss mechanism is preferred; the vehicle mechanism is characteristic of species with weaker bonding.

CHAPTER 3

POLYMER SYSTEMS

3.1 SULFONIC ACID BASED MEMBRANES

The proton exchange membrane fuel cell (PEMFC) has recently been shown to be the most promising of all the fuel cell types for applications such as automobiles, stationary power and power for small electronics such as laptop computers and cell phones (Korgesch et al., 1996). A solid polymeric membrane containing ionic groups is responsible for the proton transport from the anode to the cathode.

Polymer electrolyte fuel cells were the first type of fuel cell demonstrated in the space flight program. Originally, the proton exchange membrane (or alternatively polymer electrolyte membrane) was a sulfonated poly(styrene divinylbenzene) copolymer. These membranes showed very poor lifetimes due to oxidative degradation of the polymer backbone (Hickner, 2003).

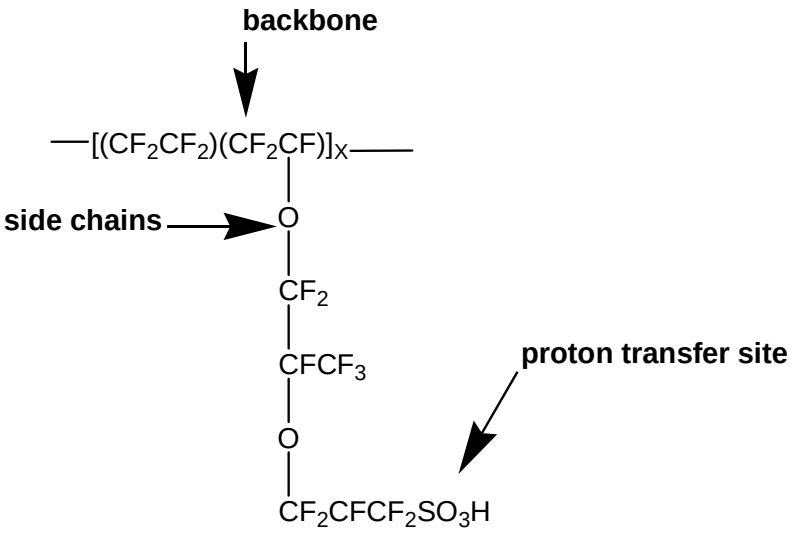

Figure 3.1 Nafion Molecular Structure.

In 1968 DuPont commercialized a proton exchange membrane based on poly(perfluorosulfonic acid) under the trade name Nafion (Grot, 1968).The highly fluorinated structure shown in Figure 3.1 displays a much greater resistanceto degradation in a fuel cell environment and thus increasingly longer fuel cell lifetimes.

Since then, other companies, such as Asahi in Japan and briefly Dow in the U.S, have investigated membranes based on poly(perflurosulfonic acid) structures, but Dow has exited the business and Asahi remains a small player. Nafion has remained the industry standard proton exchange membrane and almost all current PEM fuel cell research from a device standpoint focuses on this type of electrolyte. Major applications for Nafion also include chlorine synthesis via electrolysis (chlor-alkali processes) (Berzins, 1977).

Nafion membranes are composed of carbon-fluorine backbone chains with perfluoro side chains containing sulfonic groups (Doyle et al., 2003). The Teflon-like molecular backbone gives these materials excellent long-term stability in both oxidative and reductive environments. A lifetime of over 60,000 hours has been achieved with commercial Nafion® membranes.(Steck, 1995) These membranes exhibit a protonic conductivity as high as 0,10 S/cm under fully hydrated conditions. For a typical membrane thickness of, say, 175 μm (Nafion 117), this conductivity corresponds to a real resistance of around 0.2 Ωcm^2, i.e. a voltage loss of about 150 mV at a practical current density.

The structure model of nafion membrane which comprises ionic hydrophilic clusters, an amarphous hydrophobic region is suggested previously (Figure 3.2) (Kreuer et al., 1993). The transport properties of perfluorosulfonic membranes largely influenced by the water content of the membrane, particularly when the membrane in the acidic form. The hydrophilic cluster swells with the water content. In the dry state Nafion membrane behaves like an insulator but, when hydrated the membrane becomes conductive (Yeo et al., 1983, Pourcelly et al., 1990). Proton conductivity reaches maximum over a temperature range 55-70^oC, eventough water content is minumum. Out with these temperature ranges, the conductivity decreases resulting from deionization of the sulfonic acid groups and perhaps a change of the hopping distance between cluster zones (Rieke and Vanderborgh, 1987).

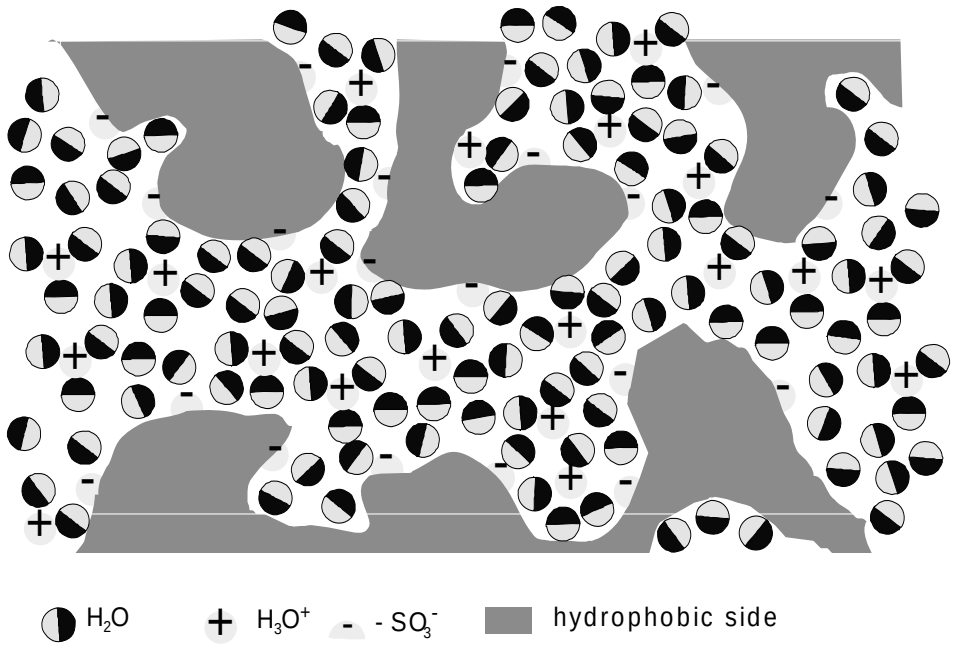

Figure 3.2 Structure model for Nafion perfluorosulfonic membrane.

Ionomer-based membranes intended for high-temperature PEMFCs should preferably retain a high conductivity at low levels of humidification. There is thus a need to improve water retention at high temperatures and to improve performance at low water contents, while simultaneously giving special attention to chemical as well as morphological stability to resist excessive water swelling. The membrane morphology is important for the performance, and is linked to the nature of the ionomer and the membrane formation process in a quite complex manner. It typically depends strongly on the water content, and on the concentration and distribution of the acidic moieties (Kreuer, 2001, Ding, 2002, Tang, 2001). For example, Kreuer has shown that hydrated membranes based on sulfonated polyetherketone have a less pronounced separation into hydrophilicyhydrophobic domains, as well as a larger distance between the acidic moieties, as compared to the Nafion membrane (Kreuer, 2001, Jannasch, 2003).

Perfluorinated PEMs have been developed by modification of the acid group (Hogarth and Glipa, 2001, Kotov et al., 1997). Thus, DesMarteau replaced the sulfonic acid group ($-SO_3H$) in Nafion with a sulfonyl imide group ($-SO_2NHSO_2CF_3$), which results in an increase in the water uptake while Kotov et al. developed membranes with a phosphonic acid group that has the potential for higher thermal stability (DesMarteau,

1995, Savett, 2002 and Kotov et al., 1997). Other perfluorinated PEMs include Gore-select which uses a PTFE matrix embedded in the perfluorinated PEM to provide mechanical strength, thus allowing membrane thickness to be reduced to below 20 mm. These membranes possess conductivity up to 0.01- 0.1 S/cm depending on RH (Liu et al., 2001).

Partially fluorinated PEMs such as the sulfonated trifluorostyrene membranes have also been developed (Hogdon, 1968). Ballard Power Systems has developed BAM3G, a family of PEMs with equivalent weights 375 to 920, by incorporating a,b,b-trifluorostyrene monomer, and a series of substituted a,b,b-trifluorostyrene comonomers. These membranes are less expensive than Nafion and have demonstrated good stability (>15,000 h) (Steck and Stone, 1997).

The majority of the new ionomers developed currently are based on different arylene main-chain polymers, which are characterized by excellent thermal, chemical, and mechanical properties. Some of these ionomers are shown in Figure 3.3. Several research groups are working with different sulfonated polymers containing diarylsulfone units (Wang et al., 2002, Poppe et al., 2002 and Jönissen et al., 2002). For example, Wang et al. have prepared high molecular weight polysulfones containing randomly distributed disulfonated diarylsulfone units.

Analysis of the membrane morphology by atomic force microscopy revealed hydrophilic phase domains that increased in size, from10 to 25 nm, with increasing degree of sulfonation. The membranes were stable up to 220^{o}C in air, and highly sulfonated ones showed conductivities of 0,17 S cm^{-1} 30 ^{o}C in water (Wang et al., 2002).

Poppe et al. have produced flexible PEMs based on carboxylated and sulfonated poly(arylene-co-arylene sulfone)s (Poppe et al., 2002). As expected, the carboxylated materials showed lower water uptake and lower conductivity in comparison with the sulfonated ones. Sulfonated polysulfones have also been blended with basic polymers such as polybenzimidazole (PBI) and poly(4-vinyl pyridine) in order to improve the performance in direct methanol fuel cells (Jönissen et al., 2002).

Different sulfonated aromatic polyimides are also under investigation (Guo et al., 2002, Genies et al., 2001, Mercier et al., 2001 and Besse et al., 2002). These ionomers typically reach high levels of conductivity, but the hydrolytic stability is reported to be very sensitive to the chemical structure of the polyimide main-chain(Genies et al., 2001, Mercier et al., 2001). A membrane-electrode assembly based on a sulfonated polyimide was recently evaluated in a fuel cell at 70^{o}C, and was found to have a performance similar to Nafion (Besse et al., 2002).

Sulfonated PBI has been investigated by Kawahara et al. and Asensio et al. (Kawahara et al., 2000, Rikukawa et al., 2000 and Asensio et al., 2002). At low water contents, PEMs of PBI grafted with sulfopropyl units showed a proton conductivity in the order of 10^{-3} S cm^{-1} in the temperature range from 20 to 140 ^{o}C, which is superior to Nafion under the same conditions (Kawahara et al., 2000). The performance of these PEMs have also recently been investigated in fuel cells at temperatures up to 150 ^{o}C under fully humidified conditions (Bae et al., 2002).

As the operation temperature of the PEMs is increased to temperatures above 100 ^{o}C, desulfonation, i.e. loss of the sulfonic acid unit though hydrolysis, becomes an increasingly important problem. Acidic moieties having higher stability include phosphonic acid and sulfonimides. The latter is a significantly stronger acid compared to sulfonic acid, which may be especially advantageous at low water contents. Allcock et al. have prepared different poly(aryloxyphosphazene)s functionalized with phenyl phosphonic acid units with the intended use in direct methanol fuel cells (Allcock et al., 2002). Just recently, the same authors also report on the preparation of poly(aryloxyphosphazene)s having sulfonimide units (Hofmann et al., 2002). Blending and radiation crosslinking have been investigated as means to reduce water swelling and methanol permeation of poly(aryloxyphosphazene) ionomers (Carter et al., 2002).

Two different polymer membrane systems based on Nafion and Teflon were investigated as proton conductors for polymer membrane fuel cells (Sun et al., 2001). Water-free Nafion117 membranes swollen with different non-aqueous solvents were prepared. The solvents included imidazole, imidazole–imidazolium salt solutions, room temperature molten salts and molten salt–acid solutions. Teflon films were treated with a surfactant, or a Nafion solution, to improve their surface properties, and were subsequently swollen with phosphoric acid. Conductivity measurements were carried

out on both the Nafion and Teflon membranes. The Nafion membranes swollen with the imidazole–imidazolium salt solutions exhibited a conductivity in the range of 3–4x10^{-3} S/cm around 100°C. This method of producing water-free systems for PEMFC membranes is therefore promising although conductivities need to be improved significantly. For the Nafion membranes swollen with the molten salts or molten salt–acid solutions, their conductivity is not as high as expected, which may be because the molten salts are not very hydrophilic, and could not play an effective role in disassociation of protons from the sulfonyl groups attached to Nafion backbones. The Teflon films treated with the surfactant solution or the Nafion solution presented good compatibility with phosphoric acid, and the Teflon membrane–phosphoric acid systems also exhibited good conductivity at higher temperatures. Further investigation on these systems should include a study of thermal stability and electrochemical stability, as well as testing in a fuel cell device (Sun et al., 2001).

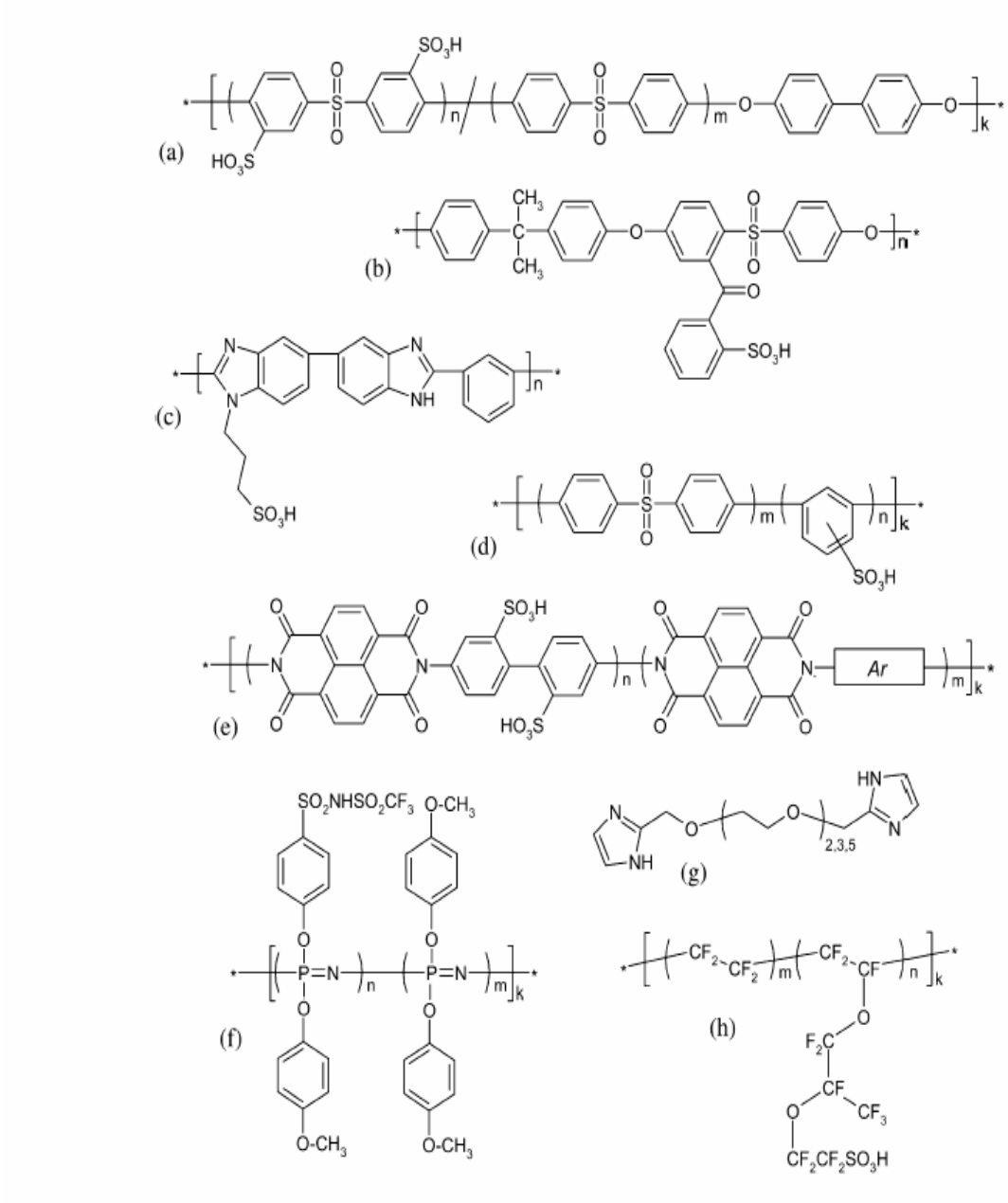

Figure 3.3 Examples of proton conducting polymers currently under investigation as PEM materials: (a) sulfonated poly(arylene ether sulfone) (Wang et al., 2002) (b) sulfophenylated polysulfone (Jannasch et al., 2002); (c) sulfopropylated PBI (Kawahara et al., 2000, Rikukawa et al., 2000; (d) sulfonated poly(arylene-co-arylene sulfone) (Poppe et al., 2002); (e) sulfonated naphthalenic polyimide (Ar, various aromatic moieties) (Genies et al. 2001); (f) poly(aryloxyphosphazene) having sulfonimide units(Hofmann et al., 2002); (g) imidazole-terminated ethylene oxide oligomers (Meyer et al., 2001); and (h) Nafion marketed by the DuPont company.

3.2 POLYMER /ACID COMPLEXES

Several research groups are currently developing high temperature PEMs based on complexes of strong acids, such as H_3PO_4 and H_2SO_4 with different basic polymers. The property of phosphoric acid to interact via hydrogen bonds facilitates the preparation of blends with a large variety of polymers. In the case of basic polymers, proton transfer from phosphoric acid to the polymer helps for a wide miscibility of these complexes. However, the miscibility limits of phosphoric acid-polymer blends are often unknown, and some of the systems reported in the literature in reality may be inhomogeneous.

Phosphoric acid is a weak acid (pKa = 2.16) (Lide, 1995) that melts at 42^{o}C in the pure state and acts as an oxidant at elevated temperatures. With basic polymers, phosphoric acid undergoes hydrogen bond interactions or proton transfer reactions. In regard to its conductivity, phosphoric acid differs from water and many other solvents in two ways. First, conductivity is remarkably high in the pure state (Chin et al., 1989). Second, when strong electrolytes (e.g., H_2SO_4) are added, conductivity decreases rather than being improved (Munson et al., 1967). The first feature is due to the generation of charge carriers by self-dissociation ($5H_3PO_4 = 2H_4PO^+_4 + H_2PO^-_4 + H_3O^+ + H_2P_2O^{2-}_7$, where H_3PO_4 = 16.8 M, $H_4PO^+_4$ = 0.89 M, $H_2PO^-_4$ = 0.43 M, $H_3O^+ = H_2P_2O^{2-}_7$ = 0.46 M at 311 K) (Dippel et al., 1993, Munson 1964) and the fact that proton migration almost entirely results from structure diffusion (Dippel et al., 1993). The second feature is also closely related to the transport mechanism. The electrical field of extrinsic charge carriers causes a bias on hydrogen bonds and thus suppresses fluctuations within the dynamical hydrogen bond network (Kreuer 1996, Kreuer 2000). Addition of water, however, increases conductivity, which passes through a temperature-dependent maximum at compositions of 45 to 60% of H_3PO_4 (Chin et al., 1989).

3.2.1 P-4VI/H_3PO_4

Poly(4-vinylimidazole), P-4VI, and phosphoric acid blends are reported (Bozkurt and Meyer, 2001).The number of moles of phosphoric acid per polymer repeat unit, x, was varied from $0 \leq x \leq 2$. These blends can be cast into homogeneous films. These blends

are chemically stable up to about 150°C. The softening temperature of the blends decrease from 77°C for x=1 to -8°C for x=2.Bozkurt and Meyer, 2001 was found the DC conductivity increases with x and reaches ~10^{-4} S/cm for x=2 at ambient temperature.

3.2.2 PEO/H_3PO_4

PEO/H_3PO_4 complexes (x= 0,42–0,66) were described in 1988 by Donoso et al., who found conductivities of 2.5 x10^{-4} S cm^{-1} at 50°C (x= 0,42) governed by segmental motion of the polymer chains. Przyluski et al. reinvestigated these blends covering a wider range of compositions (0,06 ≤ x ≤ 2,8) by means of differential scanning calorimetry (DSC), IR, Vogel-Fulcher-Tamman (VFT), and impedance spectroscopy and found VFT behavior for small x and Arrhenius behavior for larger x. The molar amount of acid per mol of polymer repeating units is described by x.

3.2.3 PEI/H_3PO_4

PEI/H_3PO_4 blends (x ≤ 0,5) were introduced by Daniel et al., 1988, who found conductivities of 1 to 3x 10^{-3} S cm^{-1} at 100°C. At x = 0,35, a precipitate was formed from the aqueous solution, which redissolved upon further addition of H_3PO_4 (x = 0,58). Schoolman et al. characterized blends of higher acid contents (x ≤ 2) that were applied as electrolytes for electrochromic devices. Whereas these researchers used branched commercial PEI, Tanaka et al. compared branched and linear PEI and found somewhat higher conductivities for the latter; however, compared with the results from Daniel et al., conductivities of the branched materials were about two orders of magnitude lower, which was attributed to the different preparation and purification procedures (Daniel et al., 1988, Schoolman et al., 1992).

Composition-dependent conductivities of branched and linear PEI blends (Daniel et al., 1988, Tanaka et al., 1995) exhibited a local maximum at $x \approx 0,2$ and dropped to a minimum at $x \approx 0,4$, where the formation of PEI-H^+. 1/2 HPO_4^{-2} was completed (the maximum degree of protonation of PEI is ~ 80%) (Bloys and Staverman, 1974). This behavior is in accordance with a maximum Tg of the blend (Daniel et al., 1988, Lassegues et al., 1989) and the precipitation from aqueous solution (Daniel et al.,1988) at $x \approx 0,35$. At higher acid levels, conductivity increased again and achieved values of

1,4 x 10^{-3}S/cm^{-1} (*l*PEI, *x* = 2,05; 100°C)(Tanaka et al., 2000). Properties of the hygroscopic, deliquescent linear PEI blends could be improved by crosslinking, which moderately influences conductivity at high x, but nearly reverses its dependence on composition at low x (Tanaka et al., 2000).

3.2.4 PAAM/H_3PO_4

PAAM/H_3PO_4 blends showed relatively high conductivities ($4x10^{-3}$ S/cm, 20°C, x=2). However, condensation of the amide groups was observed at 100°C in dry air (Rodriguez et al., 1993).

3.2.5 PBI/ H_3PO_4

In 1995, a blend of poly(benzimidazole) and phosphoric acid was considered for hydrogen fuel cell and direct methanol fuel cell (DMFC) applications for the first time (Wainright et al., 1995). PBI is an amorphous (Singleton et al., 1967, Buckeley et al.,1988), basic polymer (benzimidazole:pKa = 5.5) (Lide, 1995) of extraordinary thermal stability and a glass transition temperature of about 430°C (Singleton et al., 1967, Gilham,1972). Qingfeng et al. found that the conductivity of PBI–H_3PO_4 complexes was insensitive to humidity, but strongly dependent on the acid content, reaching values of 0.13 S cm^{-1} at 160 °C and high acid-doping levels (Qingfeng et al., 2001). It was also shown that the water drag due to proton transport was almost zero in these PEMs. Wasmus et al. used solid-state NMR characterization of H_3PO_4 doped PBI to show that the phosphoric acid sorbed by the PBI membrane was relatively immobile as compared to free phosphoric acid and revealed that there was an interaction between imidazole groups of PBI and phosphoric acid (Wasmus et al., 1995). Glipa et al. confirmed proton transfer from H_3PO_4 to the imino groups of PBI and the presence of undissociated H_3PO_4 at high doping levels with IR spectroscopy (Glipa et al., 1999). Li et al. measured conductivity as a function of temperature and a wide range of acid doping levels (x=3.0~16.0, where x is acid molecule per polymer repeat unit) at R.H. between 80%~85%. They obtained a conductivity of 4.6×10^{-2} S/cm at 165°C. They

suggested a useful H_3PO_4 doping level between 3.5~7.5, considering both conductivity and mechanical strength (Li et al., 2001). Kawahara et al. prepared H_3PO_4 doped PBI membranes by immersing the PBI membranes into a mixed solution of acid and methanol. The highest doping level observed was 2.9mol H_3PO_4/repeat unit. Based on FTIR data, they concluded that H_3PO_4 did not protonate the imidazole groups of PBI but interacted by hydrogen bonding between the OH and N groups. The presence of HPO_4^{2-} and $H_2PO_4^{-}$ anions, based on FTIR, implied that the proton conduction occurred according to the Grotthuss mechanism. The conductivity of the anhydrous PBI2.9H_3PO_4 complex reached 10^{-4} S/cm at 160°C. Fontanella et al. measured the isobaric conductivity data of PBI6H_3PO_4 membrane at temperatures of 25, 50, 75°C. Based on the activation volume values (4~7 cm^3/mol), they proposed that proton transport in the acid doped PBI was mediated by segmental motions of the polymer (Fontanella et al., 1998). Pu, et al. proposed that proton transport in phosphoric acid blended PBI was the consequences of the two contributions: one was based on rapid proton exchange (hopping) via hydrogen bonds between solvent molecules, which could be the phosphate, N-heterocycles of PBI and water molecules; and the other was based on the self-diffusion of phosphate moieties and water molecules (vehicle mechanism). They studied the temperature and pressure dependence of the conductivity of PBIxH_3PO_4 membranes (x=1.8~3.8) (Pu et al., 2002). Compared with the established Nafion™ membranes, PBI is superior in several critical properties. PBI was reported (Savadogo and Varela, 2001) to be about 100 times cheaper than Nafion at present PBI is exclusively produced by celanese, who offer only complete membrane electrode assemblies (MEA) for operating temperatures of up to 200°C. Singleton et al. claim a considerably higher mechanical strength of doped PBI than that of Nafion (Singleton et al., 1967, Wainright et al., 1995).

3.3 POLYMER/HETEROCYCLE HYBRID MATERIALS

3.3.1 Polymer Composite Materials

3.3.1.1 PVPA-Heterocycle Composite Material

Yamada and Honma have prepared the acid–base composite materials by mixing of a strong phosphonic acid polymer poly(vinylphosphonic acid) (PVPA) with the high proton exchange capacity and an organic base heterocycle, such as imidazole (Im), pyrazole (Py), and 1-methylimidazole (MeIm)(Figure 3.4). This PVPA-heterocycle composite material exhibited a large proton conductivity of $7x10^{-3}$ S cm^{-1} at 150 ^{o}C under anhydrous condition. Additionally, the thermal stability of composite material was found to increase with the mixing ratio of the heterocycle.

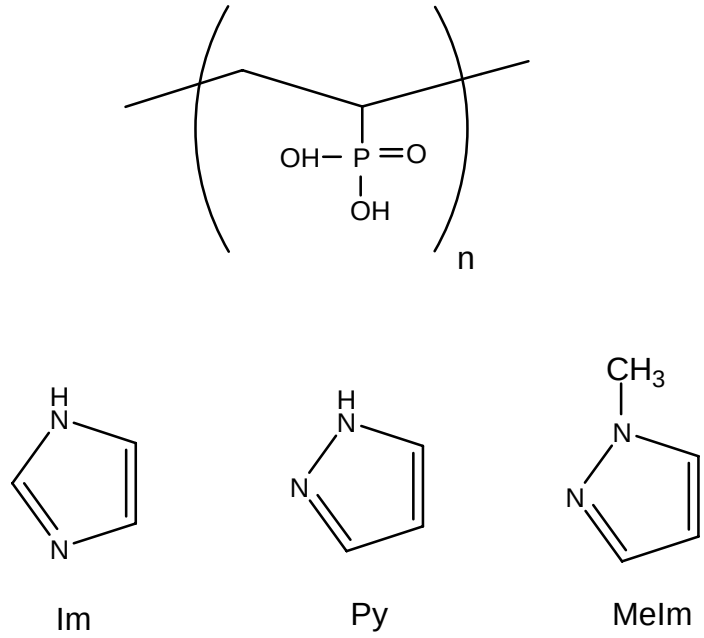

Figure 3.4 Molecular structures of poly(vinylphosphonicacid) (PVPA) , imidazole (Im), pyrazole (Py), and 1-methylimidazole (MeIm).

Anhydrous proton conductivity of PVPA-heterocycle composite materials showed differences of approximately one order of magnitude, depending on the molecular structure of basic heterocycles. These different conductivities of composite materials are due to the pKa value of heterocyclic molecules. The pKa values of heterocycle molecules (Acheson, 1976) and the maximum proton conductivity at 150 ^{o}C under anhydrous condition are listed in Table 3.1. The basicity of heterocycle molecules of Im is larger than that of Py (see the pKa1 value in Table 3.1). Clearly, the conductivity of PVPA-Im composite material is larger than PVPA-Py composite material. These results

suggest that pyrazole molecule with the low basicity do not act as a proton donor and acceptor in composite material since the free proton from the PVPA molecule could not strongly interacts with non-protonated –N═group of pyrazole ring. In contrast, the pKa1 value of MeIm molecules is as same as that of Im molecules. However, the conductivity of PVPV-MeIm composite material is lower than that of PVPA-Im. This phenomenon is due to the molecular structure of imidazole. The Im molecules have been reported the construction of molecular cluster, consisting of approximately 20 molecules (Acheson, 1976), through the intermolecular hydrogen bonding.

As a result, PVPA-Im composite material might possess fast proton transfer of inter-heterocycle molecules in the composite material. However, MeIm molecules do not construct the molecular cluster with the intermolecular interaction in membrane and cannot provide fast proton transfer kinetics in inter heterocycle molecules. Based on the basicity and clustering mechanism, PVPA-Im composite material are supposed to possess the highest proton conductivity of $7x10^{-3}$ S cm^{-1} at 150 ^{o}C under anhydrous condition in many different types of PVPA-heterocycle composite materials. These results suggest that the basicity and molecular structure of heterocycle in acid-base composite material are important factors to obtain the anhydrous proton conductivity at the intermediate temperature condition(Yamada and Honma, 2005).

Table 3.1 Maxmimum proton conductivities of PVPA-heterocycle composite material and acid dissociation constant (pKa values of various heterocycle molecules).

PVPA-heterocycle	Maximum conductivity [a] (S cm^{-1})	Pka value of heterocycle[b]	
		Pka1	pka2
PVPA-Im	7 x 10^{-3}	7.2	14.5
PVPA-Py	8 x 10^{-4}	2.5	14
PVPA-MeIm	1 x 10^{-3}	7.4	

[a] maxmimum proton conductivity 150^{o}C under anhydrous condition

[b] Referans (Acheson, 1976)

3.3.1.2 PAA/Imidazole

In 2003, anhydrous proton conducting polymer electrolytes have been prepared by entrapping imidazol (Im) in polyacrylic acid (PAA) with various stoichiometric ratios, x, to form PAAxIm (x is the number of moles of Im per polymer repeat unit) (Meyer et al., 2003). Polymer electrolytes, PAAxIm (with x = 0.5 and 1) can be cast into transparent, homogeneous films which are thermally stable up to 200 ^{o}C. From FT-IR spectra it is evident that hydrogen bonds exist between protonated and unprotonated Im units (Figure 3.5). With increasing Im content the glass transition temperature decreases while their conductivity increase, reaching 10^{-3} S/cm at 120 ^{o}C.

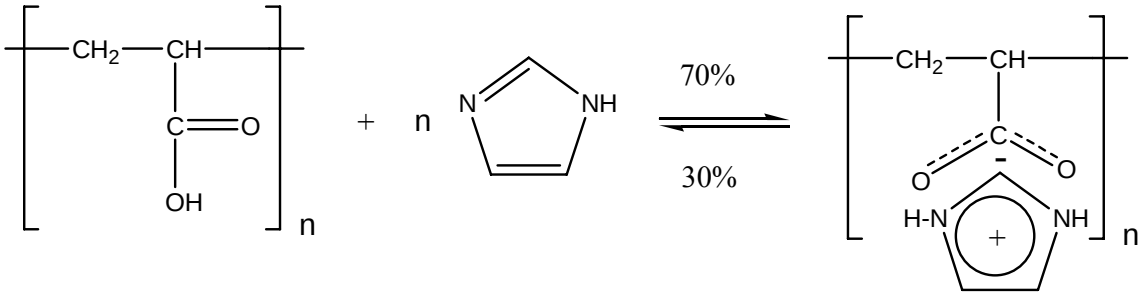

Figure 3.5 Illustration of the protonation of imidazol upon blending with PAA.

It was previously mentioned that the membrane materials based on carboxylic acid groups shows no significant proton conductivity even at higher level of hydration. Because –COOH groups are less sensitive to hydrolysis and higher pKa values (Kreuer, 1996).

The intercalation of imidazol with different doping ratio, x into PAA as Brønstedt acid increased the conductivity PAAxIm membranes. The reason may be imidazol, like water, acts as proton donor and acceptor in the proton conduction process. In this sense it behaves amphoteric but with respect to other compounds they are more basic than water (Kreuer, 1998). FT-IR of PAAxIm confirmed that imidazol is partially protonated from “free” nitrogen side. A Grotthuss type diffusion mechanism may explain the

proton diffusion process within protonated and unprotonated heterocycles. Because the protonic defect may cause local disorder by forming (. . . Him-(HimH+)-imH. . .) configuration as discussed in the literature (Münch et al., 2001). The use of imidazol in a suitable acidic host polymer to increase the concentration of defect protons may also technological interest. Further systems like PAMPSA-imidazole are under investigation and will be communicated soon.

3.3.2 Other Composite Materials

3.3.2.1 Benzimidazole/Monododecyl Phosphate Molecular Hybrids

It had been reported that a glass-filter supported monododecyl phosphate/benzimidazole mixed material shows a high proton conductivity of $1x10^{-3}$ S/cm at T=150 ^{o}C underwater-free conditions along with a high thermal stability (Yamada and Honma, 2003). Even other acid–base hybrid materials resulted in the same anhydrous conductor at elevated temperatures (Yamada and Honma, 2004, Yamada and Honma, 2004). Kim and Honma investigated the effects of monododecyl phosphate (MDP) doping to benzimidazole (BnIm)(Figure 3.6) by IR, TG, XRD, proton conductivities. The XRD results showed new phases different from the crystal structures of MDP and BnIm, and the doping of MDP displayed the peaks of BnIm due to the extinction rule of reflection. The hybrids showed a high proton conductivity of $1x10^{-2}$ S/cm above 100 ^{o}C under a non-humidified (anhydrous) condition (Kim and Honma, 2005).

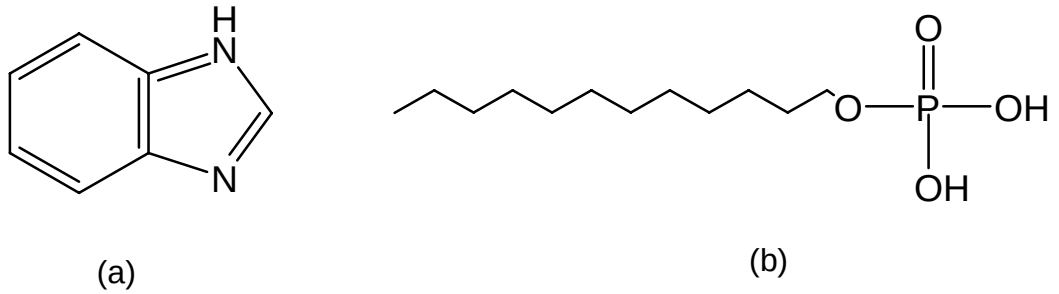

Figure 3.6 Molecular structure of (a) benzimidazole and (b) monododecyl phosphate.

3.3.2.2 Alginic Acid-Imidazole Composite Material

Other anhydrous proton conductor consisting of alginic acid (AA), one of the acidic biopolymers, and imidazole (Im) molecules, one of the basic heterocyclic molecules was reported by Yamada et al. In 2004. This AA-Im ($r \geq 20$) composite material indicated the high proton conductivity of $2x10^{-3}$ S cm^{-1} at $130^{o}C$. On the other hand, the activation energy, such as 1,2-1,6 ev, at $r \leq 1$ is extremely largen than that of other reported materials. This high activation energy is due to the long distance between the hopping sites. Additionaly, the proton hopping distance of pure AA or small mixed material ($r \leq 0,5$) was too long to hop to neighboring site, as a result, these materials could not show any measurable proton conductivity ($<10^{-8}$ S/cm)(Yamada and Honma, 2004).

The biomoleculer composite material, such as chitin phospate-hetrocyclic molecules composite materials as an anhydrous proton conducting membrane was reported by (Yamada and Honma 2004). In these cases, the composite materials showed the high proton conductivity of $\geq 10^{-3}$ S/cm at $150^{o}C$ under anhydrous condition. Additionally, these materials had a high thermal stability. However, AA-Im composite materials did not indicate the satisfactory conductivity and thermal stability in comparision with the reported materials (Yamada et al., 2003, Yamada et al., 2004). One of the reasons might be the effect of pKa value (pKa=3.1) of –COOH group in AA (Jang et al., 1996). Phosphonic acid is stronger carboxylic acid. The phosphonic acid group and basic group forms a strong acid-base complex in the composite membrane, as a result the free proton from phosphonic acid strongly interacts with non-protonated –n=(Yamada et al., 2003, Yamada et al., 2004). However a weak acid, such as –COOH group in AA, cannot form the strong acid-base in composite membrane and not provide enough mobile-protons to Im molecules, so that AA-Im composite showed the lower anhydrous proton conductivity than the phosphonic acid composite materials (Yamada and Honma, 2004).

3.3.2.3 Adipic Acid/Benzimidazole Hybrid Electrolytes

Bozkurt et al. investigated several blends of a diacid, adipic acid (AA) and heterocyclic base, benzimidazole (BnIm)(Figure 3.7). Adipic acid has very low proton conductivity (~10^{-11} S/cm) in crystalline form. The conductivity of the blends increased with BnIm and reached a maximum conductivity of $4x10^{-3}$ S/cm at 130^{o}C (Karadedeli et al., 2005).

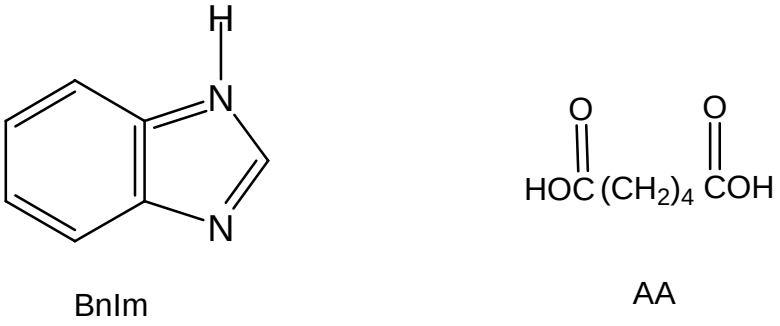

Figure 3.7 Moleculer structure of BnIm and AA.

From DSC results, it can be concluded that such conductivity increase within this temperature regime may be the effect of first-order transition (melting) onto the ionic conductivity of the samples. At higher temperatures, (T>373 K) the conductivities of these samples are very close to each other irrespective of their BnIm content. High BnIm doping levels ($BnIm_2AA$) result in higher conductivity even at lower temperatures. This behavior may reflect the ambivalent role of hydrogen bonding as already observed for the proton mobility in heterocyclic systems (Kreuer et al., 1998). Previously the proton conductivity in anhydrous heterocycles, i.e. imidazole and pyrazole, and their mixtures with H_2SO_4 and H_3PO_4 were investigated (Kreuer et al., 1998 and Schuster et al., 2003).

The protonic defects are created by protonation of heterocycles which act as solvent for protons and it is the dynamics of these solvent molecules which lead to the mobility of the protonic defects, i.e. intermolecular proton transfer and structural reorganization by hydrogen bond breaking and forming processes (structure diffusion). IR spectra of the BnImxAA indicates the partial protonation of benzimidazole which occurs from the free N side forming benzimidazolium ion. Therefore, at higher

temperatures, protons can be rapidly transferred to neighbor molecule with a small activation energy. Similar behavior was observed in PAA-imidazole and mono-dodecylphosphate (MDP)-benzimidazole mixed materials (Bozkurt et al., 2003 and Yamada et al., 2003). The BnImxAA blends showed a maximum conductivity of $4x10^{-3}$ S/ cm at 130 ^{o}C in anhydrous state. The materials which comprise $–CO_2H$ acidic functional groups as part of their constitutional unit have not been preferred as proton conductors since these units are less sensitive to hydrolysis, have higher pKA values and hence yield low conductivity. This work was demonstrated that anhydrous, high proton conductive organic electrolytes can also be obtained when $–CO_2H$ containing materials are doped with benzimidazole (Karadedeli et al., 2005).

3.3.2.4 Anhydrous Proton Conductive Membrane Consisting of Chitosan

Other anhydrous proton conducting membrane using a composite of chitosan, one of the basic biopolymers with an amino group, and methanediphosphonic acid (MP), which possesses a large proton Exchange capacity was prepared by Honma and Yamada, in 2005 (Figure 3.8).This chitosan–MP composite material showed the high proton conductivity of 5×10^{-3} S cm^{-1} at 150 ^{o}C under anhydrous (water-free) conditions. The proton conducting mechanism of the chitosan–MP composite material was due to proton transfer to the proton defect site without the assistance of diffusible vehicle molecules. The utilization of a biopolymer, such as chitosan, for PEMFC technologies is novel and challenging where biological products are usually considered as waste, non-hazardous, and environmentally benign. Especially, the low production cost of the biopolymer is an attractive feature. Anhydrous proton conducting biopolymer composite membranes may have potential not only for PEMFCs operated under anhydrous conditions, but also for bio-electrochemical devices including an implantable battery, bio-sensors. Additionally, the thermal stability of this composite material was found to increase with the mixing ratio of the MP molecule (Yamada and Honma, 2005).

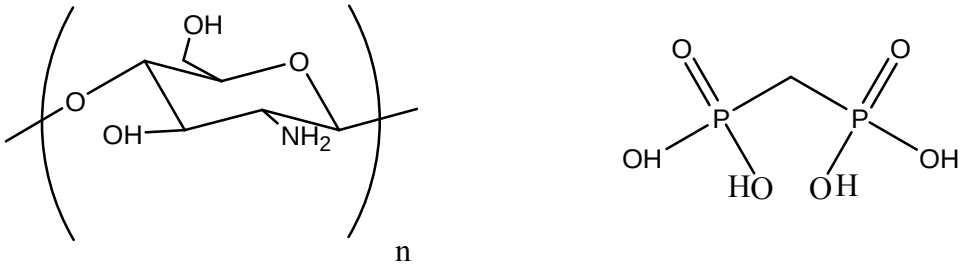

(a) (b)

Figure 3.8 Molecular structures of chitosan (a) and methanediphosphonic acid (b)(MP).

CHAPTER 4

APPLICATION OF PROTON CONDUCTING ELECTROLTES FUEL CELLS

Fuel cells are electrochemical devices that convert chemical energy into electrical and thermal energy using various fuels, such as natural fuels, hydrocarbons, and hydrogen. The history of the fuel cell dates back to 1839 when William Grove, a British amateur physicist, first discovered the fuel cell principle. He used four large cells that contained both hydrogen and oxygen to produce electricity that was then used to split the water in the upper cell into hydrogen and oxygen.the basic physical structure

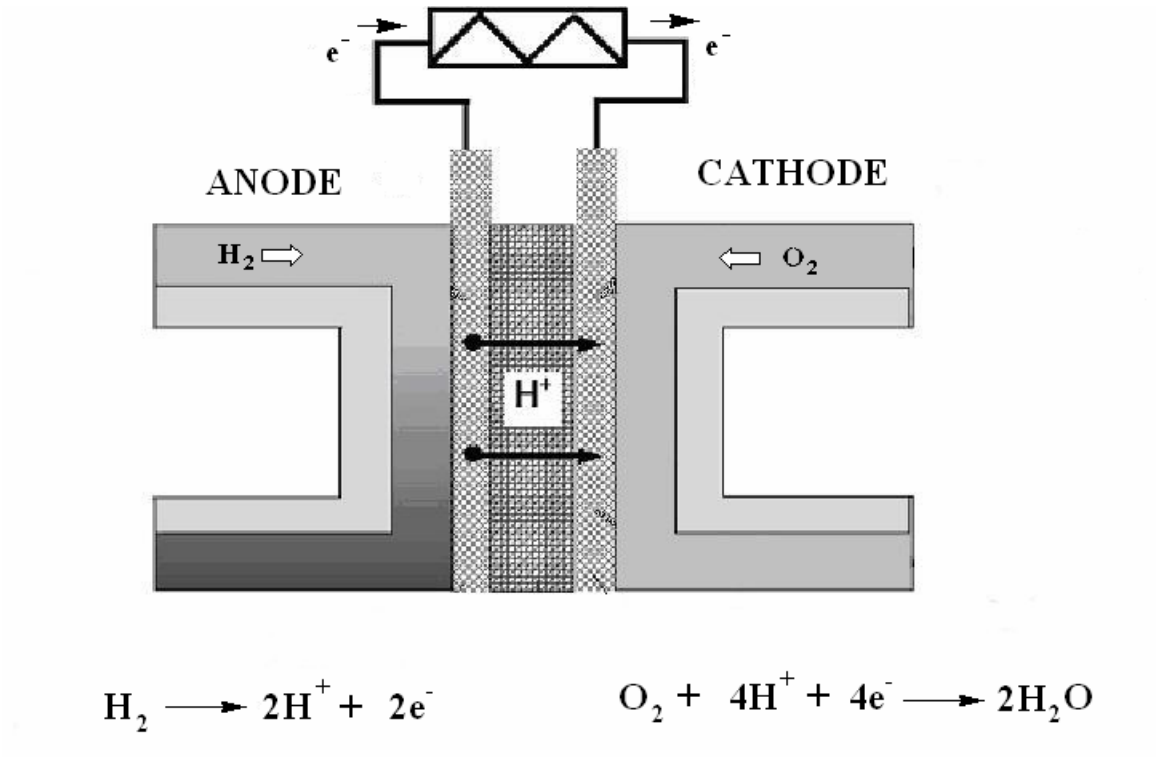

Figure 4.1 Schematic of an Individual Fuel Cell.

or building block of a fuel cell consist of an electrolyte layer in contact with a porous anode and cathode either side. A schematic representation of a fuel cell with the reactant / product gases the ion conduction flow directions through the cell is shown in Figure 4.1.

In a typical fuel cell, gaseous fuels are fed continuously to the anode (negative electrode) compartment and oxidant (i.e., oxygen from air) is fed continuously to the cathode (positive electrode) compartment; the electrochemical reactions take place at the electrodes to produce an electric current. A fuel cell, although having components and charecteristics similar to those of a typical battery, differs in several respects.The battery is an energy storage device. The maximum energy available is determined by the amount of chemical reactant stored within the battery itself. The battery will cease to produce elecrical energy when the chemical reactants are consumed (i.e., discharged). In a secondary battery, the reactants are regenerated by recharging, which involves putting energy into the battery from an an external source. The fuel cell, on the other hand, is an energy conversion device that theoretically has the capability of producing elecrical energy for as long as the fuel and oxidant are supplied to the electrodes.In reality, degradation, primarily corrosion, or malfunction of components limits the practical operating life of fuel cells.

The electrolyte not only transports dissolved reactants to the electrode, but also conduct ionic charge between the electrodes and thereby completes the cell electric circuit.It also provides a physical barrier to prevent the fuel and oxidant gas streams from directly mixing.

The functions of porous electrodes in fuel cells are : 1) to provide a surface site where gas /liquid ionization or de-ionization reactions can take place, 2) to conduct ions away from or into the three-phase interface once they are formed (so an electrode must be made of materials that have good electrical conductance), and 3) to provide a physical barrier that separates the bulk gas phase and electrolyte.

A variety of fuel cells are in different stages of development. They can be classified by use of diverse categories, depending on the combination of type of fuel and oxidant, whether the fuel is processed outside (external reforming) or inside (internal

reforming) the fuel cell, the type of electrolyte, the temperature operation, whether the reactants are fed to the cell by internal or external manifolds, etc. The most common classification of fuel cells is by the type of electrolyte used in the cells.

4.1 PHOSPHORIC ACID FUEL CELLS (PAFCs)

PAFCs generate electricity at more than 40 % efficiency, and nearly 85 % of the steam this fuel cell produces is used for cogeneration. Operating temperatures are in the range of 150-200^{o} C. At lower temperatures, phosphoric acid is a poor ionic conductor, and carbon monoxide (CO) poisoning of the platinum (Pt) electro-catalyts in the anode becomes severe. The electrolyte is liquid phosphoric acid soaked in a matrix. One of the main advantages to this type of fuel cell, besides the nearly 85% cogeneration efficiency ,is that it can use impure hydrogen as fuel. PAFCs can tolerate a CO concentration of about 1.5 percent, which broadens the choice of fuels they can use. If gasoline is used, the sulfur must be removed.Disadvantages of PAFCs include: it uses expensive platinum as a catalyst, it generates low current and power comparably to other types of fuel cells, and it generally has a large size and weight.

4.2 PROTON EXCHANGE MEMBRANE FUEL CELLS (PEMFCs)

These cells operate at relatively low temperatures (about 80^{o} C), have high power density, can vary their output quickly to meet shifts in power demand, and are suited for applications, such as in automobiles, where quick start up is required. They are the primary candidates for light-duty vehicles, for buildings and potentially for much smaller applications such as replacements for rechargeable batteries. The proton Exchange membrane is a thin plastic sheet that allows hydrogen ions to pass through it. The membrane is coated on both sides with highly dispersed metal alloy (mostly platinum) that are active catalysts. The electrolyte used is a solid organic polymer polyperflourosulfonic acid. The solid electrolyte is an advantage because it reduces corrosion and management problems. Hydrogen is fed to the anode side of the fuel cell where the catalyst encourages the hydrogen atoms to release electrons and become hydrogen ions (protons). The electrons travel in the form of an electric current that can

be utilized before it returns to the cathode side of the fuel cell where oxygen has been fed. At the same time, the protons diffuse through the membrane (electrolyte) to the cathode, where the hydrogen atom is recombined and reacted with oxygen to produce water, thus completing the overall process. This type of fuel cell is, however, sensitive to fuel impurities.

4.3 MOLTEN CARBONATE FUEL CELLS (MCFCs)

These fuel cells use a liquid solution of lithium, sodium and /or potassium carbonates, soaked in a matrix for an electrolyte. They promise high fuel-to-electricity efficiencies, about 60 % normally or 85 % with cogeneration, and operate at about 650^{o}C. The high operating temperature is needed to achieve sufficient conductivity of the electrolyte. Because of this high temperature, noble metal catalysts are not required for the cell' s electrochemical oxidation and reduction processes. MCFCs have been operated on the hydrogen , carbon monoxide, natural gas, propane, landfill gas, marine diesel, and simulated coal gasification products. The high operating temperature serves as a big advantage because this implies higher efficiency and the flexibility to use more types of fuels and inexpensive catalysts as the reactions involving breaking of carbon bonds in larger hydrocarbon fuels occur much faster as the temperature is increase a disadvantage to this, however, is that high temperatures enhance corrosion and the breakdown of cell components.

4.4 SOLID OXIDE FUEL CELLS (SOFCs)

Another highly promising fuel cell, this type could be used in big, high-power applications including industrial and large-scale central electicity generating stations. Some developers also see SOFC use in motor vehicles and are developing fuel cell auxiliary power units (APUs) with SOFC s. A solid oxide system usually uses a hard ceramic material of solid zirconium oxide and a small amount of ytrria, instead of a liquid electrolyte, allowing operating temperatures to reach 1000^{o}C. Power generating efficiencies could reach 60 % and 85 % with cogeration.

Alkaline fuel cells can achieve power generating efficiencies of up to 70 percent. They were used in Apollo spacecraft to provide both electricity and drinking water. Their operating temperature is 150 to 200^{o}C. They use an aqueous solution of alkaline potassium hydroxide soaked in a matrix as the electrolyte. This is advantageous because the cathode reaction is faster in the alkaline electrolyte, which means higher performance.

4.5 DIRECT METHANOL FUEL CELLS (DMFCs)

These cells are similar to the PEM cells in that they both use a polymer membrane as the electrolyte. However, in the DMFC, the anode catalyst itself draws the hydrogen from the liquid methanol, eliminating the need for a fuel reformer. Efficiencies of about 40 % are expected with this type of fuel cell, which would typically operate at a temperature between 50-100^{o}C. This is relatively low range, making this fuel cell attractive for tiny to mid-sized applications, to power cellular phones and laptops. Higher efficiencies are achieved at higher temperatures. A major problem, however, is fuel crossing over from the anode to the cathode without producing electricity.

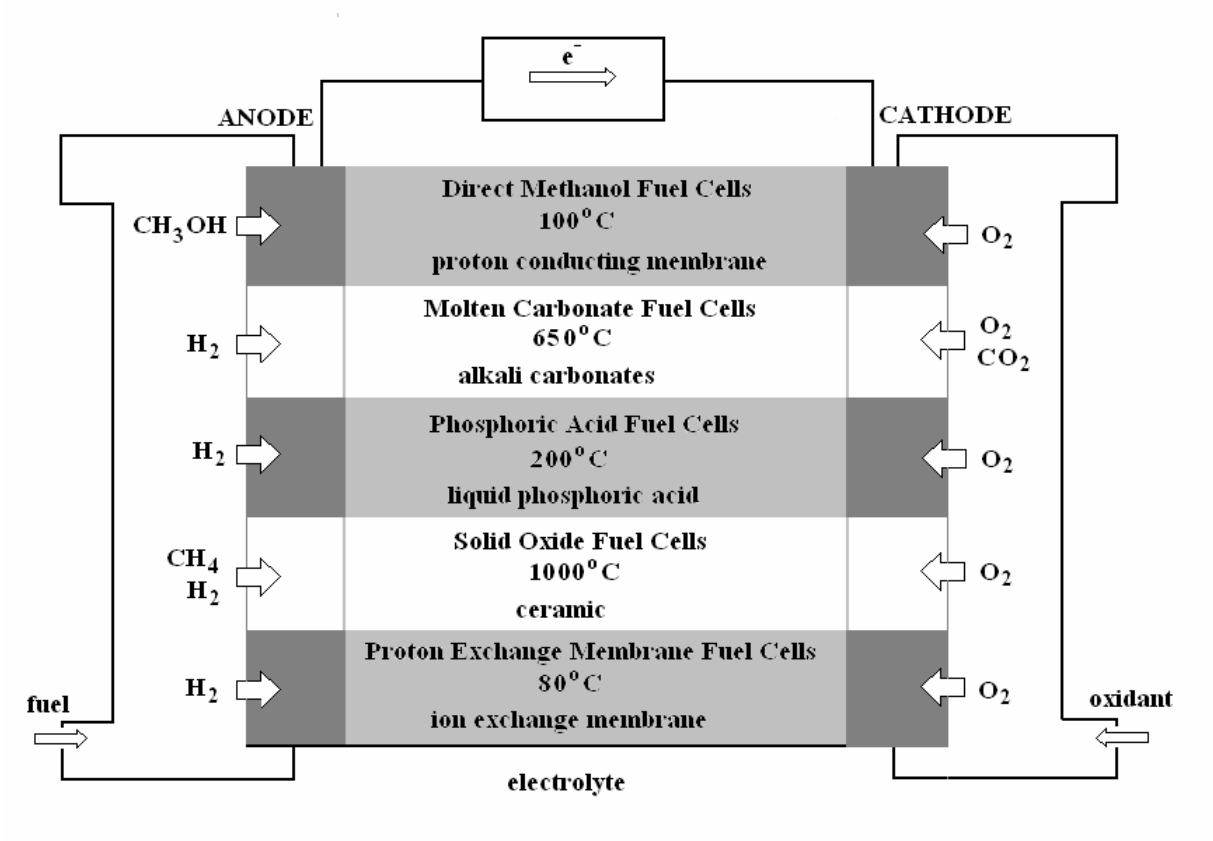

Figure 4.2 Overview of the different types of fuel cells. Temperature values indicate the maximum operating temperature.

CHAPTER 5

EXPERIMENTAL

5.1 PURPOSE AND PREVIEW

To prepare novel anhydrous proton conducting polymer electrolytes satisfying the following requirements :

a) Wide thermal stability window (at least 150K)

b) Sufficient ionic conductivity (>10^{-5} S/cm)

c) Thermodynamic stability and electrochemical stability

With this aim in mind the following results needed to be achieved :

i) Proton conducting polymer blends working in a wide temperature range have been prepared.

ii) Thermal stability of the polymers were examined by TGA.

iii) Thin polymer blend films were prepared with different ratios.

iv) The polymer-base interactions were investigated via their IR spectra.

v) Homogenity of the films was analyzed by DSC.

vi) Conductivity measurements were performed using impedance spectroscopy within the 10^{-1} to 10^{6} Hz frequency region.

5.2 CHEMICALS

Polyethleneglycol-hexacarboxylic acid (PEG-HCA) were obtained from organic chemistry research group at Fatih University, has an average molecular weight 1036 g/mol. The chemical structures of PEG-HCA are shown in Figure 5.1.

Ethyleneglycol methacrylate phosphate (EGMP) (Figure 5.2) was provided by Aldrich and used without futher purification.

Imidazole (IM) (>99,5) with melting point 88-91^{o}C has molecular weight 68,06g/mol, is obtained from Aldrich.

Benzimidazole (BnIm) with melting point 172^{o}C has a molecular weight 118,14 g/mol , is obtained from Aldrich.

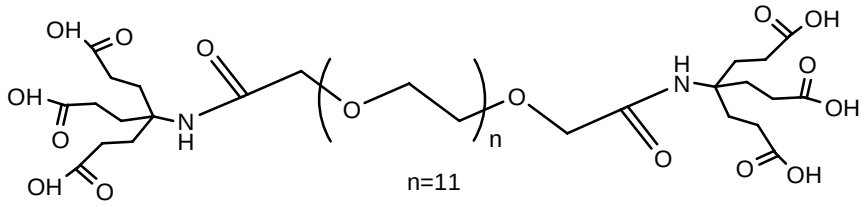

Figure 5.1 Structures of Polyethleneglycol-hexacarboxylic acid (PEG-HCA).

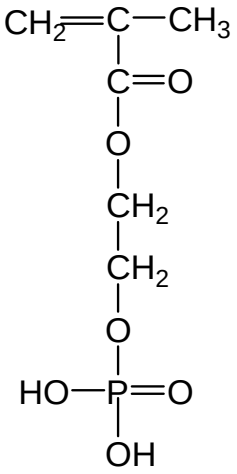

Figure 5.2 Structure of the Ethyleneglycol methacrylate phosphate.

5.3 PREPARATION OF POLYMER BLENDS

5.3.1 Preparation of the PEG-HCA xIm

A stoichiometric amount of PEG-HCA and Im were mixed in THF and the resulting mixture was stirred overnight. Solutions with x ranging from 0.5 to 1.0 were prepared where x is the number of moles of imidazole per moles of –COOH unit. From these solutions, gels were cast on polished, polytetrafluoroethylene (PTFE) plates and dried under vacuum at 60^{o}C. The quantities of PEG-HCA/ Im in THF use as solvent to

achieve the mixing ratio x are summarized in Table 5.1. Figure 5.3 shows structures of PEG-HCA xIm blends.

Table 5.1 PEG-HCA and Im amounts to obtain the ratio x.

X	PEG-HCA	Im	THF(ml)
0.5	10g (9.66 mmol)	1.97g (28.98 mmol)	40
1	10g (9.66 mmol)	3.94g (57.96 mmol)	40

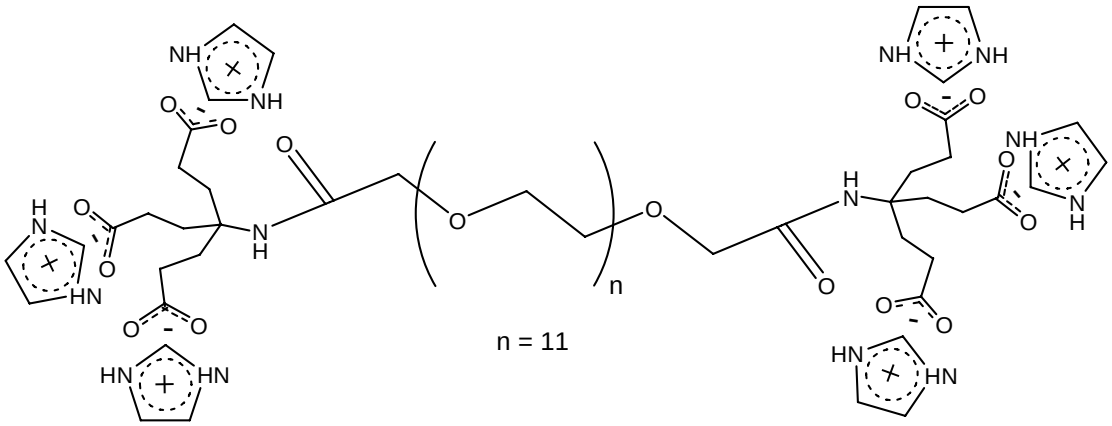

Figure 5.3 Structures of PEG-HCA xIm.

5.3.2 Preparation of the homopolymer

In a 100 ml three-necked flask required amount of 5 g of Ethylene glycol methacrylate phosphate (EGMP) (23,8 mmol) was dissolved in 30 ml THF. 0,039 g of AIBN (0,238mmol) was added to the solution. The mixture was stirred for 3 h under N_2 atmosphere at 60 ^{o}C using a magnetic stirrer. This mixtures was washed with THF(x2) and then was dried under vacuum. Thus, solid, white, powder homopolymer was produced.

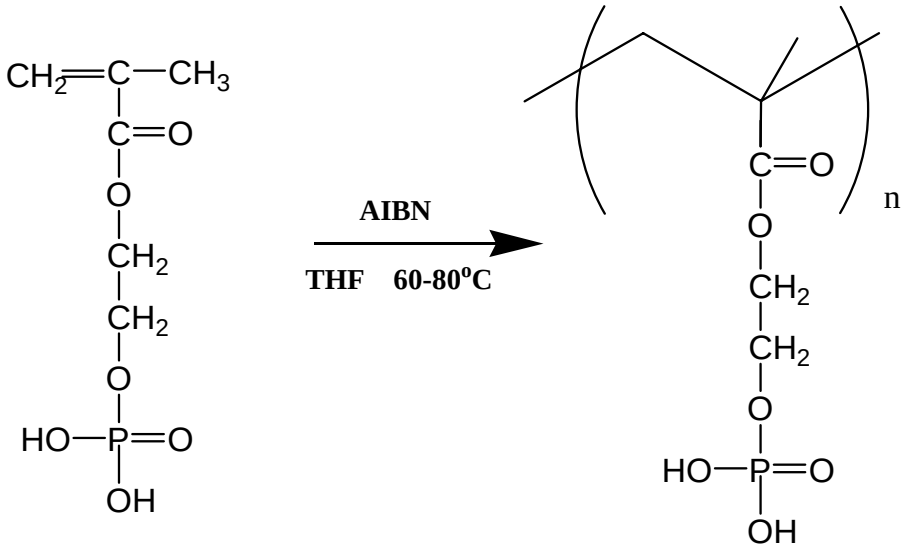

(5.1)

EGMAP **PEGMAP**

5.3.3 Preparation of the Poly(EGMAP-Im$_X$)

The polymer electrolytes were prepared by free radical bulk (thermal) polymerization of EGMAP using AIBN as initiator. The composite electrolyte Poly(EGMAP-Im $_x$) with x=1 was prepared by mixing of 2 g (9.52 mmol) of the monomer Ethylene glycol methacrylate phosphate (EGMAP) with 0,65g (9,53 mmol) of imidazole (IM). The viscous solution was stirred at least two hours under dry conditions and 0.016 g of AIBN (1 mol % of the monomer) was dissolved. The solution was transferred to PTFE plates and polymerized under N_2 atmosphere at 85 ^oC for 36 hours. The products were washed with excess THF and dried under vacuum.

Table 5.2 EGMAP and IM amounts to obtain the ratio x.

X	EGMAP (g)	IM (g)
0,5	2	0,32
0,75	2	0,49
1	2	0,65
1,5	2	0,98

5.3.4 Preparation of the Poly(EGMAP-BnIm$_X$)

The composite electrolyte Poly(EGMAP-BnIm$_x$) with x=1 was prepared by mixing of 2 g (9.52 mmol) of the monomer Ethylene glycol methacrylate phosphate (EGMAP) with 1,13 g (9,55 mmol) of benzimidazole (BnIm). The viscous solution was stirred at least two hours under dry conditions and 0.016 g of AIBN (1 mol % of the monomer) was dissolved. The solution was transferred to PTFE plates and polymerized under N_2 atmosphere at 85 ^oC for 36 hours. The products were washed with excess THF and dried under vacuum.

5.4 INSTRUMENTATION AND PROCEDURE

TGA Thermal stabilities of polymers and doped electrolytes were investigated by Perkin Emler Pyris 1 and by TGA Mettler-Toledo TG50, respectively. The samples (-10 mg) were heated with a rate of 10^{o}C/min under N_2 atmophere from room temperature to 700^{o}C under an inert atmosphere. Weight loss was measured and reported as a function of temperature.

DSC data were obtained between -150/+150^{o}C using Mettler- Toledo DSC 30 insrument. The samples are weighted (10-15mg) and loaded into aluminum pans and slowly cooled from room temperature to starting temperature. Samples were then heated to desired temperature with a scan rate of 10^{o}C/ min (Run I). In Run II samples were slowly coolede 60-70 ^{o}C below their glass transition temperature then heated to desired temperature. The second heating curves are evaluted. Empty aluminum pans are used as a reference.

Elemental analyses were done by laboratory of Research&Development-Training Center of Middle East Technical University (METU) Central Laboratory which is a soot of the the scientific and technical research council of Turkey.

Ion exchange capacity (IEC) of the composite materials were measured by placing them in 2 M NaCl solution overnight to exchange all the H^+ with Na^+. The proton content in the salt solution was determined by titration with NaOH solution of known concentration. The IEC was calculated according to:

IEC (meq/g) = C (mmol/cm^3) V_{NaOH} (cm^3) /w_{dry} (g)

where C is concentration of NaOH, V_{NaOH} is the volume of NaOH and w_{dry} is the mass of dried sample (Rikukawa et al., 2005).

FT-IR spectra of the samples were recorded by depositing a thin film onto silicon wafers. The IR spectra (4000-400 cm^{-1} with resolution of 4 cm^{-1}) have been recorded with Matson Genesis II spectrometer. Complexation of PEGMAP with Im and BnIm at stoichiometric ratios x was recorded by this technique.

The AC conductivities of the samples were measured in the Max-Plank Institute for Polymer Research using a Novocontrol impedance spectrometer in the frequency range from 1Hz to 1 MHz as a function of temperature. The hot pressed pellets of the samples with a diameter of 10 mm and thickness of about 0.2-0.3 mm were sandwiched between two gold-coated electrodes and their conductivities were measured with 10 ^{o}C intervals under dry-nitrogen atmosphere. The DC conductivities were derived from the AC conductivities measurements.

CHAPTER 6

CHARACTERIZATION OF PROTON CONDUCTING POLYMER ELECTROLYTES

6.1 FT-IR

FT-IR spectroscopy is a powerful tool for structure elucidation.The position, intensity, and shape of vibrational bands are useful in clarifying conformational and environmental changes of polymers at the molecular level.

FT-IR has found particularly wide application in the field of the polymer analysis, not only because of the ability to look at intractable, thick, intensely absorbing materials but also because of the ability to observe chemical and physical changes in the polymer structure with the admixture of the additives (Compell and White, 1989).

6.1.1 FT-IR of PEG-HCAxIm

The spectra of PEG-HCAxIm is represented in Figure 6.1. Normally , C=O stretching of carboxylic acid group gives strong peak near 1730 cm^{-1}. The same group shows a medium peak at 1280 cm^{-1} corresponding to in plane deformation of C–O–H and at 1185 cm^{-1} due to –(C–O)H stretching. Subsequent to blending of the PEG-HCA with imidazole, a new broad peak appears at 1653cm^{-1} and the intensity of the carbonyl stretching at 1730 cm^{-1} decreased for x=0.5 and completely disappeared with x=1.The former peak arises from the asymmetric stretching of deprotonated carboxylic acid units. These occur by the transfer of the acidic proton of the carboxylic acid to the ‘‘free’’ nitrogen side of imidazole to form imidazoliumion (Figure 6.1). A broad peak between 3400 and 3000 cm^{-1} is attributed to hydrogen bonding network formation.

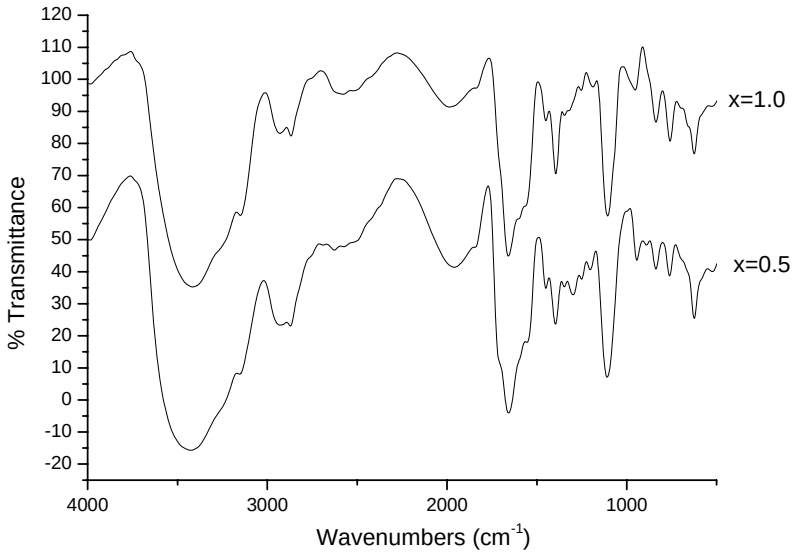

Figure 6.1 FT-IR spectra of the PEG-HCAxIm.

6.1.2 FT-IR of Poly(EGMAP-Im$_X$)

FT-IR spectra of the homopolymer and Poly(EGMAP-Im $_x$) (x=0.50, 0.75, 1.00 and 1.50) are represented in figure 6.2 and figure 6.3, respectively. The homopolymer (bottom spectrum) shows strong and broad bands which are centered at 1010 cm^{-1} and 1160cm^{-1} due to (P-O)H and P=O stretching, respectively. The same group gives additional broad bands near 3400-3000 cm^{-1} and 2500-2050 cm^{-1}. The absorption band at 1730 cm^{-1} is due to the stretching of C=O unit. Proton exchange reactions in Poly(EGMAP-Im $_x$) can be proved by the peak located at 1620 cm^{-1} that can be attributed to protonated imidazole ring. Additionally, one can notice the descending intensity of (P-O)H peak at 1010 cm^{-1} as well as downward shift of the same peak with increasing x (from 0.50 to 1.50). The intense peak that is located at 1056 cm^{-1} is related to the $P\text{-}O^-$ formation. Besides, the composite electrolytes show an absorption band near 3130 cm^{-1} corresponds to N-H group involved in hydrogen bonding of the protonated heterocycles.

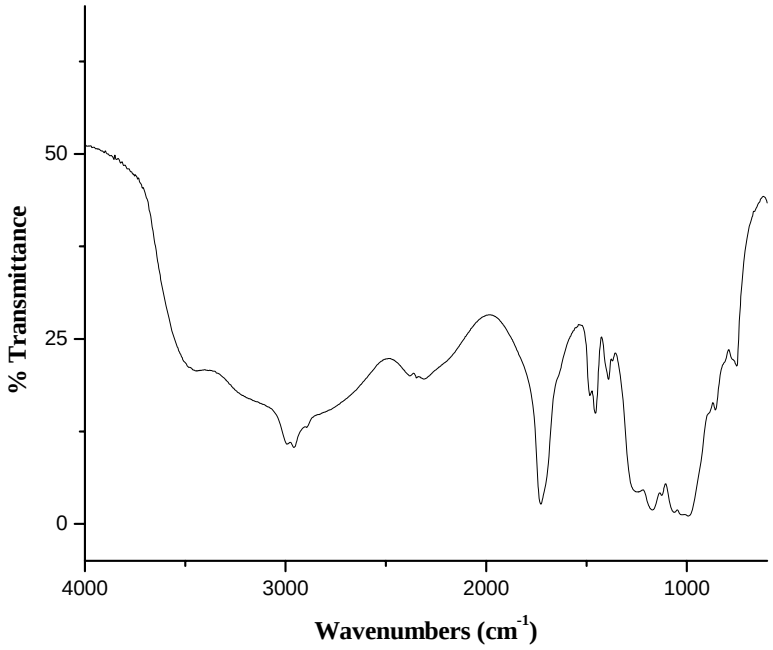

Figure 6.2 FT-IR spectra of homopolymer poly(ethyleneglycolmethacrylate phosphate).

(6.3)

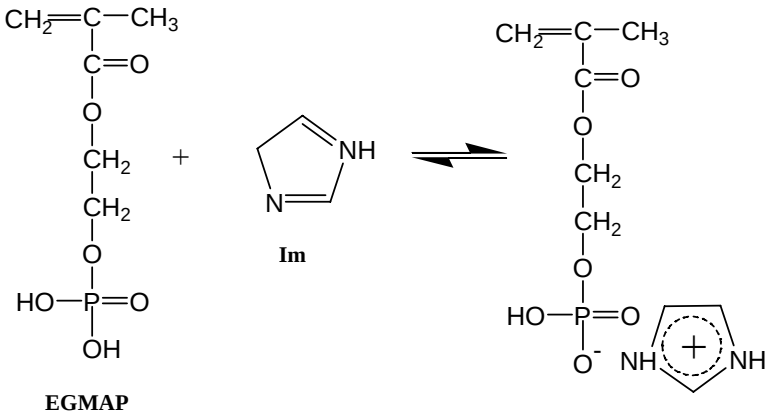

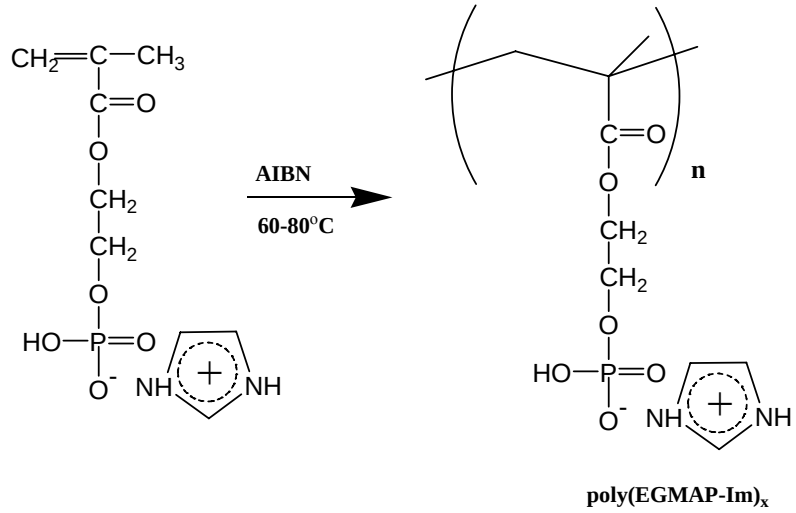

(6.3)

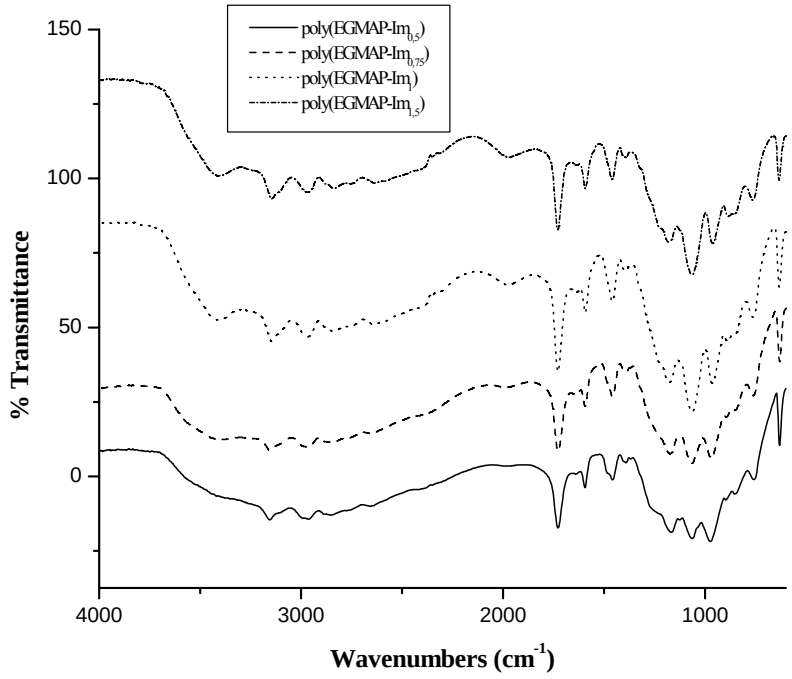

Figure 6.3 FT-IR spectra of polymers composites of EGMAP-Im_x.

6.1.3 Poly(EGMAP-$BnIm_X$)

Figure 6.4 shows the FT-IR spectra of the homopolymer and Poly(EGMAP-$BnIm_x$) (x=1). The homopolymer (bottom spectrum) shows strong and broad bands which are centered at 1010 cm^{-1} and 1160cm^{-1} due to (P-O)H and P=O stretching, respectively. The same group gives additional broad bands near 3400-3000 cm^{-1} and 2500-2050 cm^{-1}. The absorption band at 1730 cm^{-1} is due to the stretching of C=O unit. The spectra of Poly(EGMAP-$BnIm_1$) shows a peak at 1595 cm^{-1} that corresponds to

benzimidazolium ion. Additionally, one can notice the descending intensity of (P-O)H peak at 1010 cm^{-1} as well as downward shift of the same peak with increasing x (from 0.75 to 1.0). The intense peak that is located at 1056 cm^{-1} is related to the $P\text{-}O^-$ formation. Besides, the composite electrolytes show an absorption band near 3130 cm^{-1} corresponds to N-H group involved in hydrogen bonding of the protonated heterocycles.

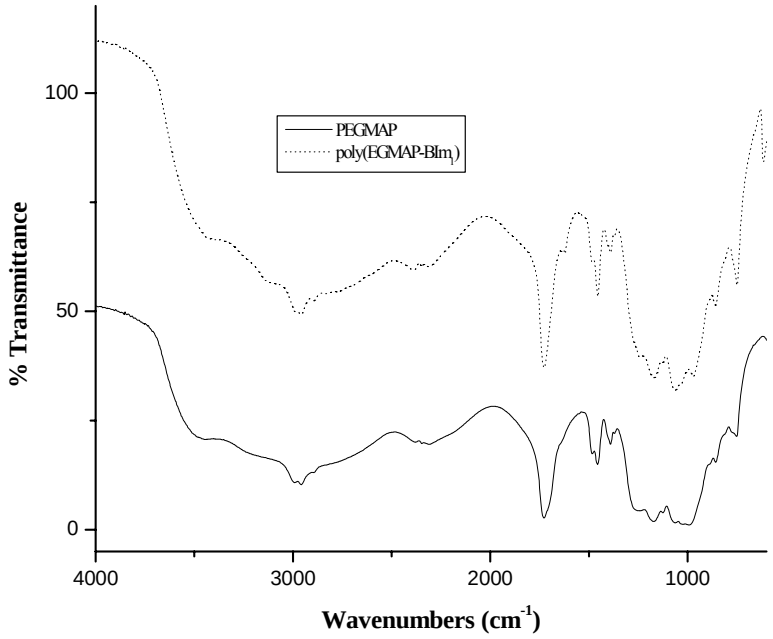

Figure 6.4 FT-IR spectra of polymers composites of EGMAP-$BnIm_x$.

(6.4)

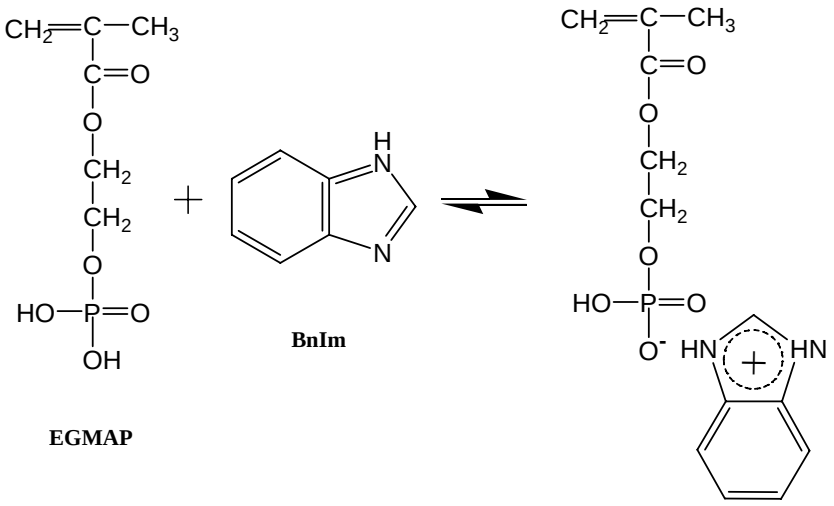

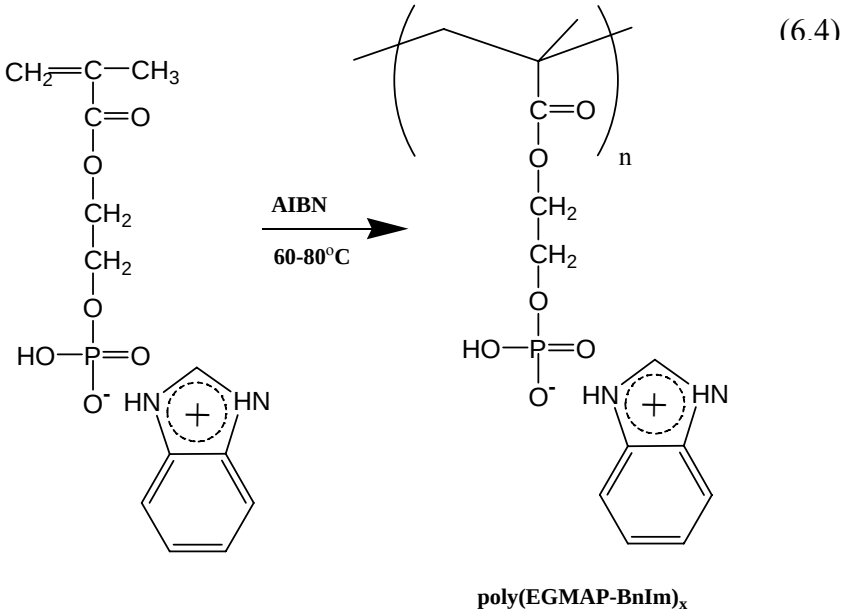

(6.4)

poly(EGMAP-BnIm)$_x$

6.2 THERMAL ANALYSIS

6.2.1 Thermogravimetric Analysis (TG)

Thermogravimetric analysis has become an indispensable analytical technique for materials characterization. It involves continuous weighing of the polymer as it is subjected to a temperature program and provides quantitative and qualitative kinetic information on the degradation, oxidation, evaporation or sublimation of material under investigation (Craver, 1983). Thermogravimetric analysis is also important for compositional analysis and determination of the additives in particular. The determination of the moisture content in polymer is also possible (Wundelich, 1990, Brennan, 1977).

6.2.1.1 TG of PEG-HCAxIm

Thermogravimetric analyses (TG) were performed under nitrogen atmosphere. The samples were dried 2 days under vacuum at 60 ^{o}C prior to measurement. For anhydrous PEG-HCAxIm complexes the initial weight reduction starts at 182 ^{o}C both

x=0.5 and *x* = 1 (Fig.6.5). The weight loss above this temperatures can be attributed to evaporation of dopant and followed with decomposition of the blends.

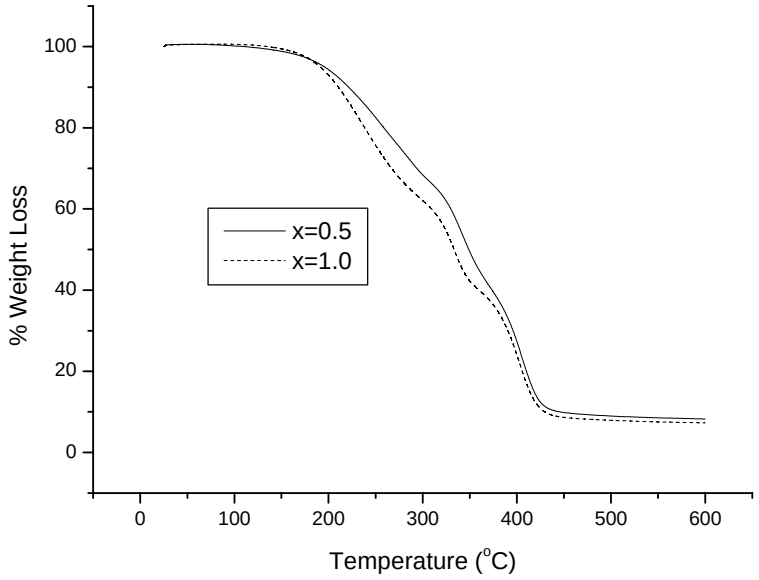

Figure 6.5 TG curves of PEG-HCAx Im recorded under N_2 atmosphere with a heating rate of 10 °C/min.

6.2.1.2 TG of Homopolymer and Composites

Thermogravimetric (TG) analysis of the homopolymer, PEGMAP and composite electrolytes, Poly(EGMAP- Im_x) and Poly(EGMAP- $BnIm_x$) are shown in Figure 6.6, 6.7, 6.8 and 6.9. The TG weight loss of the PEGMAP below 140 °C can be attributed to condensation of phosphonic acid groups. The heat treatment of the homopolymer, PEGMAP above 100 °C results in the decrease in intensity of P-OH (near 1000 cm^{-1}) in the IR spectrum that is due to formation of P-O-P groups (Fig. 6.6). Rikukawa et al. have also mentioned cross-linking reaction of the phosphonic acid groups of the EGMAP based copolymer membranes when they heat treated above 100 °C (Rikukawa et al., 2005). The composite electrolytes with x=1 illustrate an elusive weight loss in the temperature range of 160 °C to 200 °C then they decompose (Fig. 6.8 and 6.9). Additionally, the sample with a low mixing ratio (x=0.75) decomposes near 220 °C (Fig. 6.7). These results suggest that the condensation reactions of the phosphonic acid groups may be inhibited through doping with imidazole or benzimidazole.

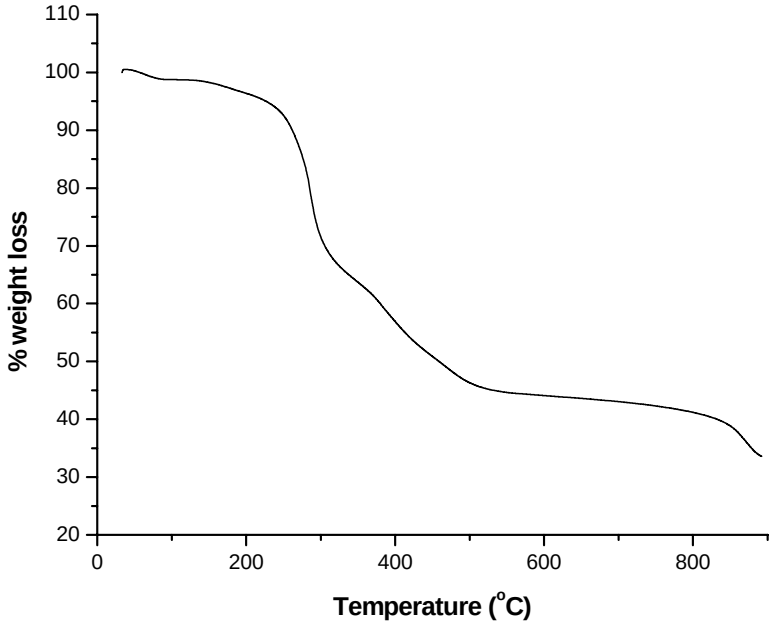

Figure 6.6 TG curves of PEGMAP recorded under N_2 atmosphere with a heating rate of 10 ^{o}C/min.

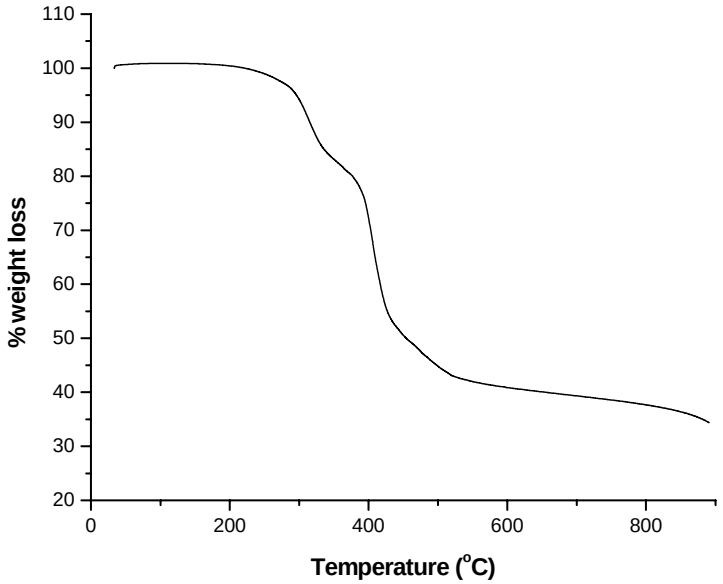

Figure 6.7 TG curves of PEGMAP-0,75 Im recorded under N_2 atmosphere with a heating rate of 10 ^{o}C /min.

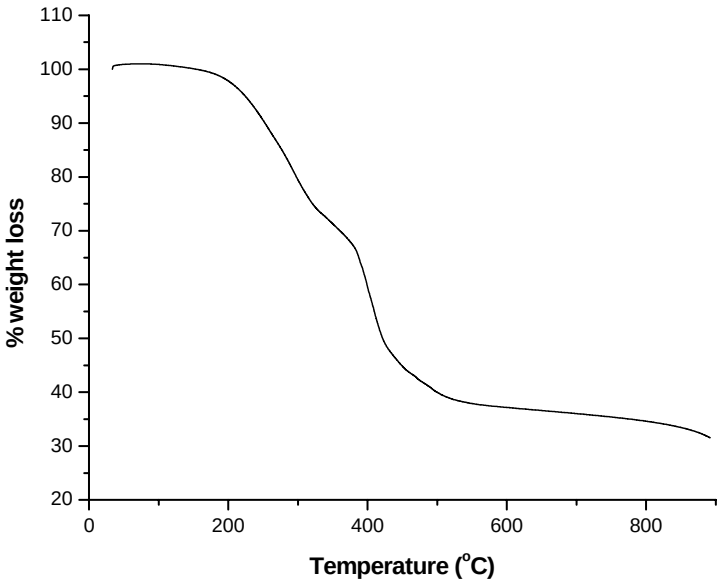

Figure 6.8 TG curves of PEGMAP-1 Im recorded under N_2 atmosphere with a heating rate of 10 ^{o}C /min.

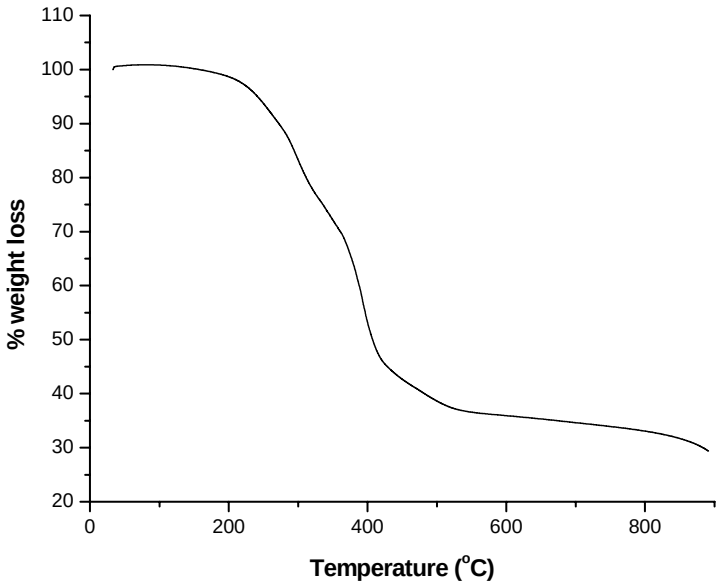

Figure 6.9 TG curves of PEGMAP-1BnIm recorded under N_2 atmosphere with a heating rate of 10 ^{o}C /min.

6.2.2 Differential scanning calorimetry (DSC)

Differential Scanning Calorimetry is most widely used methods of the thermal analysis in polymer science. They monitor the heat exchange can be physical or chemical in the nature. Polymerization or structural changes are almost invariably accompanied by energetic effects, e.i, crystallization, melting, curing and other reactions, and glass transition all show characteristic DSC curves. In the DSC, small samples (a few mg) are used and rapid heating (+q), rates up to 50-100 K/min are common. This technique is of great value for carrying out kinetic studies. Even if there are some similarities in equipment and application, DSC and DTA are different in their measurement system. In DTA, the sample and reference are heated by a single heat source with the same rate. The temperature difference between sample and reference ($\Delta T=T_s-T_r$) is measured and plotted as a function of sample temperature (T_s). The deviation of the sample temperature, T_s from T_r (ΔT) is directly proportional to the heat capacity. In DSC, the sample and reference are provided with different heaters and both sample and reference cells are kept at the same programme temperature (T_p). The temperature of each cell is measured continuously and compared with the instantaneous value of T_p. When a sample undergoes a thermal transition, the power to the two heaters is adjusted to maintain T_p and signal proportional to the power difference is plotted versus T_p.The power difference is W_s (T_s-T_p) - W_r (T_r-T_p), where the first term is the power delivered to the sample and second is power delivered to the reference (Crompton, 1989, Compbell and White, 1989).

6.2.2.1 Glass transition temperature (Tg)

Glass transition phenomenon manifest a transition from a glassy amorphous polymer to a flexible material on warming through tg. At this temperature the variables entropy, S, volume, V, enthalpy, H, merely change slope with increasing temperature. Large scale segmental motions of the polymer chain occur above this temperature. The location of Tg depends on the rate at which the temperature variation is carried out.

6.2.2.2 Variation of Glass Transition Temperatures

The Tg lowering phenomenon which can occur when a nonpolymeric liquid is incorporated into some polymers is known as plasticization. The addition of nonvolatile dioctylphtalate politicizes poly (vinyl chloride) and provides a shifting of glass transition below ambient temperature (Compbell, 1994).

6.2.2.3 DSC Studies of PEG-HCAxIm

DSC thermograms of PEG-HCAxIm are shown in Fig. 6.10. The Tg of the blend is -4^{o}C for x=0.5 and -22^{o}C for x=1. This behaviour can be explained the plasticization effect of dopant which was described in our previous work (Bozkurt and Meyer, 2001). It is clearly seen that one phase model is reasonable assumption for anhydrous PEG-HCAxIm blends. In addition the absence of melting temperature indicated that the materials are amorphous.

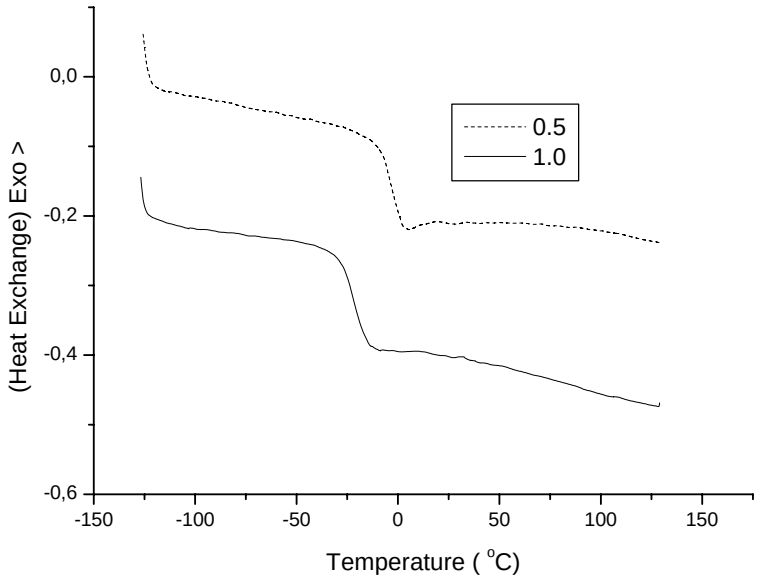

Figure 6.10 DSC curves of PEG-HCAxIm recorded under N_2 atmosphere with a heating rate of 10 ^{o}C /min.

6.2.2.4 DSC Studies of PEGMAP and Blends

DSC thermograms of the PEGMAP, Poly(EGMAP- Im_x) and Poly(EGMAP-$BnIm_x$) are represented Figure 6.11, 6.12, 6.13 and 6.14. For the homopolymer, broad initial endotherm at 50-130 ^oC was attributed to absorbed water (Kotov et al., 1997). All the composite electrolytes have almost the same softening temperature at ~50 ^oC. The slight endothermic curvature near 50 ^oC may correspond to the plasticization effect of ethylene oxide units of the EGMAP. Clearly, there is no plasticizing effect of Im or BnIm. These results imply that bulk polymerization of EGMAP in the presence of heterocycles results in crosslinked materials where the presences of ethylene oxide units may contribute to the cooperative segmental mobilities of the polymer chains.

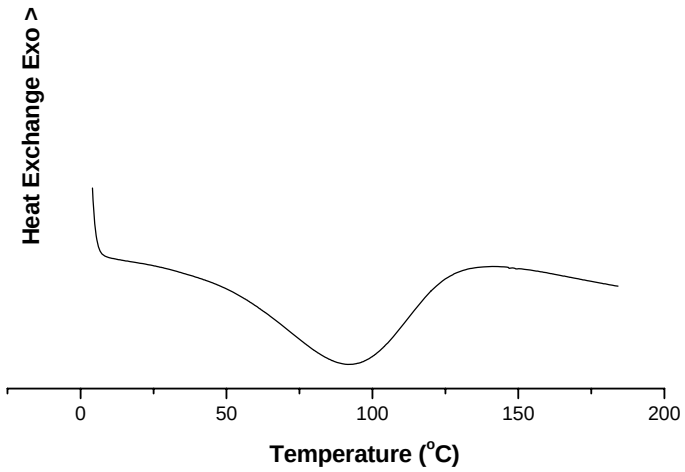

Figure 6.11 DSC curves of PEGMAP recorded under N_2 atmosphere with a heating rate of 10 ^oC /min.

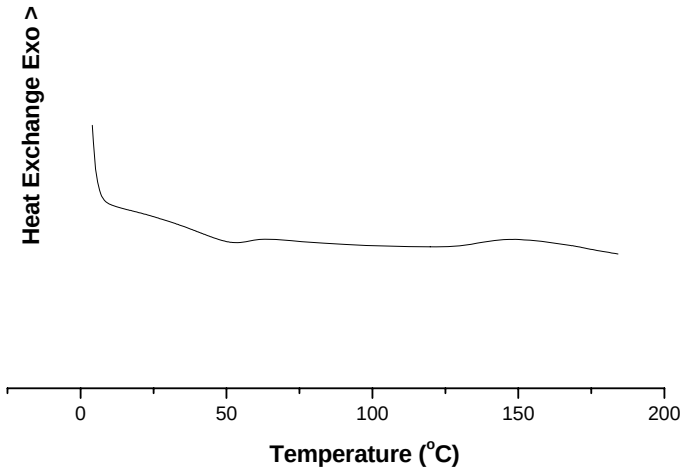

Figure 6.12 DSC curves of PEGMAP 0.75 Im recorded under N_2 atmosphere with a heating rate of 10 ^oC /min.

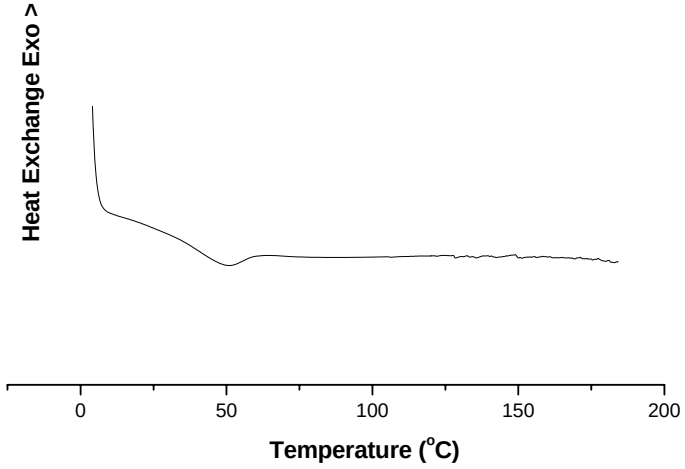

Figure 6.13 DSC curves of PEGMAP 1 Im recorded under N_2 atmosphere with a heating rate of 10 ^oC /min.

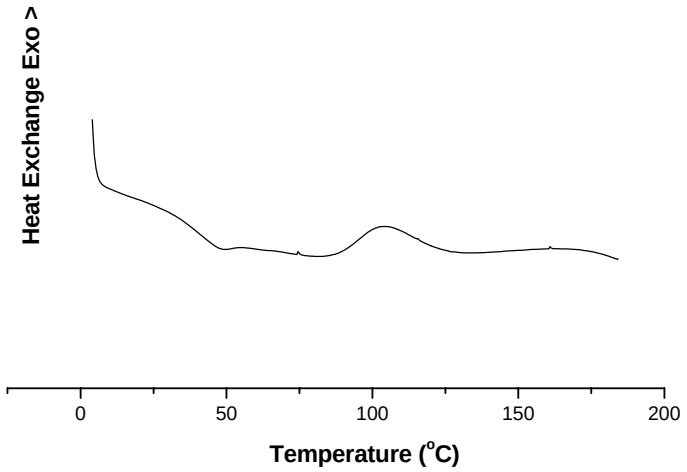

Figure 6.14 DSC curves of PEGMAP 1BnIm recorded under N_2 atmosphere with a heating rate of 10 ^{o}C /min.

6.3 ELEMENTAL ANALYSIS (EA)

The compositions of the composite electrolytes, measured by elemental analysis, are summarized in Table 6.1. The elemental analysis data (% N contents) of the composite electrolytes are consistent with compositions in the feed. For example, the found % N values by EA for Poly(EGMAP-Im_1) and Poly(EGMAP-$BnIm_1$) were 9.49 and 8.85 against the calculated values of 10.0 and 8.48, respectively. These results shows that washing with THF which is a good solvent for both monomer and heterocycles, do not influence the final composition of the materials.

6.4 ION EXCHANGE CAPACITY (IEC)

The ion exchange capacity of the homopolymer and composite electrolytes were measured (Table 6.1). Quantitatively, the IEC of the homopolymer, PEGMAP was 2.6 meq/g. This result is lower than expected and may substantiate the hypothesis of aggregation and cross-linkage of the phosphoric acid units (Rikukawa et al., 2005).

Higher IEC values of 2.9 and 3.4 meq/g were obtained for Poly(EGMAP-Im_1) and Poly(EGMAP-$BnIm_1$), respectively.

Table 6.1 % N composition and Ion Exchange capacity (IEC) the Composite materials.

Composite Electrolytes	Composition (% N)		IEC (meq/g)
	Calculated	Found by EA	
Poly(PEGMAP-Im_1)	10.0	9.49	2.9
Poly(PEGMAP-$Im_{0.75}$)	8.01	8.55	3.6
Poly(PEGMAP-$BnIm_1$)	8.48	8.85	3.4

6.5 CONDUCTIVITY OF POLYMER ELECTROLYTES

The ion conductivity in some inorganic crystals such as α- AgI, $Rb_4Cu_{11}I_7C_{13}$, ß-Alumina and Nasicon reaches values between 10^{-3}-10^{0} S/cm at ambient temperature (Takahashi, 1989, Laskar and Chandra, 1989). The mixtures of polymers with alkali metal salts have been extensively studied in the last few decades (Armand, 1983, Shriver et al., 1981, Cowie and Sadaghianizadeh, 1990). The study of PEO/inorganic salts mixtures starded from the analysis of the structure of a solid crystalline complex and it was proposed that helical PEO surrounds the cation which interacts with the lone electron pairs of the oxygen atoms. Ionenes are polyelectrolytes with N^{+}- cations as a part of their polymer repeat unit, with low molecular weight anions to balance the coulombic charges. They have been analyzed by several groups (Dominiquez and Meyer, 1988, Rietz et al., 1994). In addition to these, poly-p-phenylene sulfonate and polystyrene sulfonate are also conductive, however, only one type of ion is mobile ("single ion conductors"). These single ion conducting polyelectrolytes have ionic groups such as $–SO_3^-$, $-CO_2^-$. They conduct by the counter cations. Generally the ionic conductivities of these single ion conducting polymers are 10^{-2} S/cm that of the ordinary amorphous ion–conductive polymers because of low ionization sulfonate or carboxylate salts in comparison with $MClO_4$ or MCF_3SO_3 (M=metal ion) inorganic compounds.

Recently, a similar strategy as in polymer /salt mixtures was followed by the polymer-inorganic acid complexes in order to achieve the required proton conductivity (Przyluski and Wieczorek, 1991). The above mentioned “polymer electrolytes” and “polyelectrolytes” are known to conduct the electricity by the transport of free ions. The electrical conductivity measurement of these materials are performed with both, direct current (DC) and alternating current (AC) measurements. The former method is accomplished by sandwiching the material between two nonblocking or blocking electrodes and a DC voltage is applied. Then from the resulting current, the resistance of the sample is measured (Linford, 1990). The latter method, AC measurements, is the most popular approach for the determination of electrical properties of polymer electrolytes. In this method a sinusoidal voltage is applid to a cell which functions as a capacitor and the resulting impedance is determined. The details of the conductivity measurements by an AC experiment will be explained in the following sections.

6.5.1 AC Conductivity Measurements

The measurement of the ionic conductivity with AC impedance spectroscopy has become a standart method simply because it is possible to separate the impedance contribution form the relexation processes and eliminate the effect of the electrode polarization. The measurements are carried out within the frequency range 10^{-2}–10^{7} Hz. The sample is sandwiched between two blocking electrodes, and a sinusoidal voltage is applied to the cell (Figure 6.15).

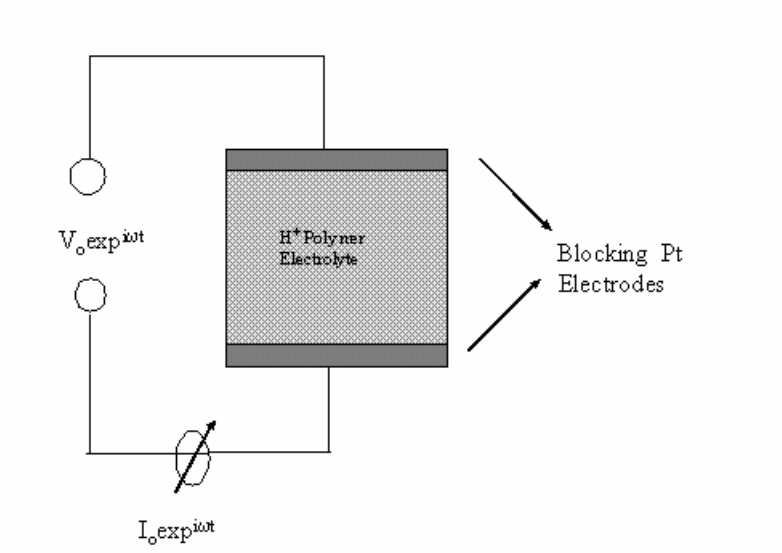

Figure 6.15 Circuit for AC impedance measurements (Blythe, 1979).

When an ac voltage is applied the frequency dependent complex dielectric constant ε* presented by (Eq. 6.3) (Blythe, 1979)

$$\varepsilon^* = \varepsilon' - i\,\varepsilon'' = \frac{C^*}{C_o} \qquad (6.3)$$

where C_o (Eq. 6.4) is the capacitance between plates in the absence of the sample.

$$C_o = \varepsilon_o \frac{A}{d} \qquad (6.4)$$

And ε_o is the vacuum permittivity ($\varepsilon_o = 8.852*10^{-14}$ F/cm) , A, and d are the area and distance between the plates respectively. The C* İs the complex capacitance with the sample. The frequency dependent voltage V (t), and current I (t) are given by (Eq.6.5);

$$I(t) = \frac{dq(t)}{dt} = \frac{d[\,C^*\,V(t)\,]}{dt} = i\omega C_o\,\varepsilon^*\,V(t) \qquad (6.5)$$

from the equations (6.3), (6.4) and the (Eq.6.5) is obtained

$$\frac{I(t)}{V(t)} = \frac{1}{Z^*(t)} = \omega C_o (\varepsilon'' + i\varepsilon) \quad (6.6)$$

It is convenient to consider the sample as being frequency dependent capacitance, C_p and the resistance, R_p in a electrically equivalent paralel circuit. The complex impedance is Z* (t) given as

$$\frac{1}{Z^*(t)} = \frac{1}{R_p} + i\omega C_p \quad (6.7)$$

and comparing the equations (6.6) and (6.7) the real and imaginary parts of ε* are obtained with paralel capacitor, C_p and R_p paralel resistor

$$\varepsilon' = \frac{C_p}{C_o} \quad (6.8)$$

$$\varepsilon'' = \frac{1}{R_p \omega C_o} \quad (6.9)$$

the loss factor (Eq. 6.10) which is related with the heat loss in the material due to the motions of the charges and dipoles is;

$$\tan\delta = \frac{\varepsilon''}{\varepsilon'} \quad (6.10)$$

and the complex conductivity is σ* (eq..6.11)

$$\sigma^* = \sigma' + i\sigma'' = i\omega\varepsilon_o\varepsilon^* \quad (6.11)$$

the frequency dependent AC conductivity, σ_{ac} is defined by (Eq. 6.12) and (Eq. 6.13)

$$\sigma(\omega) = \mathrm{Re}\,\sigma^*(\omega) \quad (6.12)$$

$$\sigma_{ac}(\omega) = \sigma'(\omega) = \varepsilon''(\omega)\,\omega\,\varepsilon_o \qquad (6.13)$$

6.5.2 DC Conductivity Measurements

Generally the observation of plateaus at low frequencies of log σ_{ac} against log ω (frequency independent values of conductivity) corresponds to DC conductivity, σ_{dc}. σ' can be written (Eq.6.14)(Chen et al., 1992, Chowdari and Gopalakrishnan, 1987).

$$\sigma' = \sigma(0) + \sigma(0)\ \frac{\omega^p}{\omega_s^p} \qquad (6.14)$$

σ (0) represents the DC conductivity when frequency is extrapolated to zero frequency (Eq. 6.15)

$$\lim_{\omega \to 0} \sigma'(\omega) \to \sigma_{dc} \qquad (6.15)$$

and ω_s is the critical frequency at which dispersion of conductivity begins and p represents the slope of the dispersion region at higher frequencies and it is related to the carrier hopping rate. The conductivity at ω_s is given by (Eq. 6.16)

$$\sigma(\omega_s) = 2\sigma(0) \qquad (6.16)$$

6.5.3 Theoretical Treatment of Ion Conduction in Solid Electrolytes

Ionic compounds and polymers can be categorized according to their conductivity: (i) *insulators* with ionic conductivity lower than 10^{-10} S/cm, (the electronic contribution to the conductivity is in the same range).(ii) *ionic conductors*; the presence of charge carries increases the conductivity up to 10^{-5} S/ cm. (iii) *superionic conductors* with conductivity of at least 10^{-4} S/cm.

6.5.3.1 Ion Conduction in Solid Electrolytes

The bulk conductivity in solid electrolytes depends on the concentration of free ions (Eq.6.17)(Reisinger, 1998). The concentrations of these charge carries and their mobilities should be high since;

$$\sigma = \sum n_i (z_i e) \mu_i \qquad (6.17)$$

n_i is the number of carries of type i, $z_i e$ is the net electronic charge on the ion or aggregate, and μ_i is mobility. The energies of activation of the formation and diffusion of these charge carries should be higher than that of potential barries to transport the ions.The ionic mobility, μ_i is related to the diffusion coefficent D_i by the Nerst – Einstein(NE) equation (Eq.6.18)

$$\mu = \frac{z_i e D_i}{kT} \qquad (6.18)$$

this yields with (Eq.6.17) the conductivity (Eq.6.19)

$$\sigma = \frac{n_i (z_i e)^2 D}{kT} \qquad (6.19)$$

The conductivity in the glassy state may sometimes be expressed by the Arrhenius equation (Eq. 6.20)

$$\sigma = \sigma_o \exp (-E_a / kT) \qquad (6.20)$$

E_a is activation energy for conductivity and σ_o is the preexponential factor.

6.5.3.2 Ion Conduction in Amorphous Polyelectrolytes

The multiphase behaviour in a material influences the ion conductivity since the presence of both, crystalline and amorphous regions introduce phase boundary effects. The ion conductivity is usually higher in the amorph region. The conductivity of the crystalline material increases rapidly when it melts. In order to understand the ionic motion in solid electrolytes, fully homogeneous amorphous polymer-salts or polyelectrolytes are considered.In this type of conductor the ion transport strongly depends on the ion duffision, which is cooperative rearrangement of the polymer segments, i.e., associated with a local free volume or viscosity of the material.

The temperature (and frequency) dependent viscosity of amarphous polymers can be described by the Vogel-Tammann-Fulcher, VTF equation (Eq.6.21) (Ratner, 1987)

$$\eta = C \exp\left(\frac{-B}{k(T-T_o)}\right) \text{ with } C \alpha T^{1/2} \qquad (6.21)$$

The empirical relationship (Doolittle eq.) (Eq.6.22) between viscosity and free volume of the material can be represented by the formula 6.22

$$\eta = A \exp\left(b_o \upsilon_o / \upsilon_f\right) \qquad (6.22)$$

b_o is a dimensionless constant, υ_o is the van der waals volume and υ_f is the average free volume. From the Stokes Einstein relation (Gauthier et al., 1988) the VTF conductivity eqution (Eq.6.23) results

$$\sigma = \sigma_o \exp\left(\frac{-B}{k(T-T_o)}\right) \qquad (6.23)$$

where T_o is the Vogel temperature generally placed ~ 50K below the glass transition temperature which is idealized as the temperature at which all " free volume " vanishes or all polymer segmental motions disappear or the configurational entropy of the material vanishes. The σ_o contains a $T^{-1/2}$ term and some other constants, B is proportional to a characteristic hard sphere volume of the moving polymer chain segment or to the inverse expansivity of the material. This equation shows the conductivity and viscosity relation as a function of temperature. The WLF (Eq.6.24) eqution includes both the viscosity and relaxation processes in amorphous systems.

$$\sigma = \sigma(T_r)\exp\left(\frac{C_1[T - T_r]}{C_2 + T - T_r}\right) \qquad (6.24)$$

where C_1 and C_2 are constant which are obtained experimentally, T_r is a reference temperature.

Both WLF and VTF equations are identical when; $C_1C_2 = B$ and $C_2 = T_r - T_o$. These two eqution offer several advantages: they describe the temperature dependent conductivity and transport properties including, viscosity and conductivity. They allow for an interpretation of several parameters such as T_o (VTF temperature) and V_f (free volume). However, they don' t give information about the microscopic structure such as molecular weight dependence of the ion transport and the mechanism of ion transport. To understand the microscopic transport the "Dynamic Bond Percolation" model was suggested for amarphous materials (Ratner, 1987). The static percolation model can be defined as the set of sides at which the moving ions can reside (hopping process). This is valid in the glassy framework of solid electrolytes. When the $T>T_g$, then the static bond percolation model can not characterize the ion motion, in this case the motion of ions occurs dynamically by means of coordinated segmental motions of the polymer host timescales.

6.5.4 Proton Conductivity in Blends of PEG-HCAxIm

The conductivity of gels of the blends cast onto platinum electrodes was determined using impedance spectroscopy in the frequency range from 10^{-1} to 10^{6} Hz and temperature range from 233 to 393 K. Figures 6.16 and 6.17 displays the frequency dependence of the alternating current, AC conductivity (σ_{ac}) of x = 0.5 and x = 1 respectively. In both samples the curves comprise the frequency independent conductivity plateau regions, which are well developed at low frequencies and at low temperatures and expand and shift toward higher frequencies with increasing temperature. The direct current, DC conductivity (σ_{dc}) of the samples is estimated from the AC conductivity plateaus. The plateau values in the medium-frequency range coincide well with DC conductivity values obtained from the *Z*' minimum in the real and imaginary (*Z*'/*Z*'') plot of impedance. Therefore, DC conductivities could be taken from the extrapolation of AC conductivity plateaus. The temperature dependence of the DC conductivities of *x* = 0.5 and 1.0 are compared in Figure 6.18. A marked curvature is observed both x= 0.5 and x= 1 with the T range of measurements. Typical curves are interpreted with the Vogel–Tamman–Fulcher (VTF) equation. It was previously mentioned that the membrane materials based on carboxylic acid groups shows no significant proton conductivity even at higher level of hydration. Because –COOH groups are less sensitive to hydrolysis and higher p*K*a values (Kreuer, 1996). The addition imidazole with different doping ratio, *x* into PEG as Brønstedt acid increased the conductivity PEG-HCAxIm membranes. The reason may be imidazole, like water, acts as proton donor and acceptor in the proton conduction process. In this sense it behaves amphoteric but with respect to other compounds they are more basic than water (Kreuer et al., 1998). FT-IR of PEG-HCAxIm confirmed that imidazole is partially protonated from "free" nitrogen side. A Grotthuss type diffusion mechanism may explain the proton diffusion process within protonated and unprotonated heterocycles. Because the protonic defect may cause local disorder by forming (. . . Him-(HimH+)-imH. . .) configuration as discussed in the literature (Münch et al., 2001) The use of imidazol in a suitable acidic liquid electrolyte to increase the concentration of defect protons may also technological interest. PEG-HCAxIm shows maximum proton conductivity of 10^{-3} S/cm for x= 1 and $8x10^{-4}$ S/cm for x= 0.5

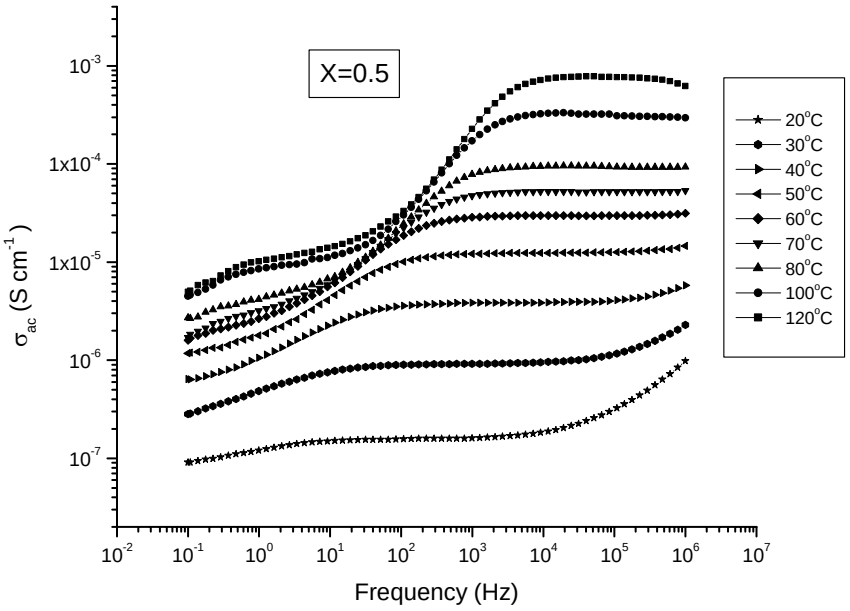

Figure 6.16 AC conductivity of PEG-HCA0.5 Im at several temperatures.

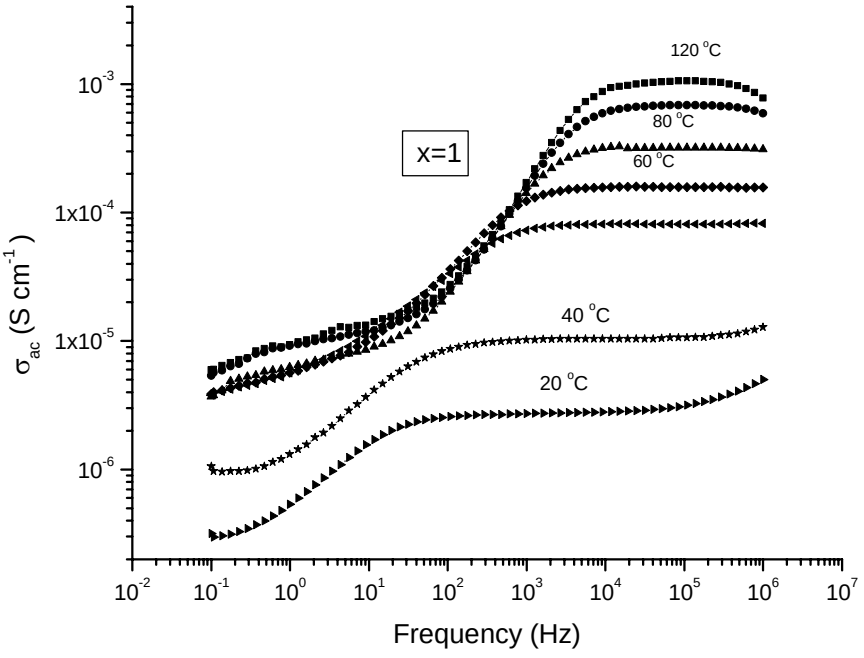

Figure 6.17 AC conductivity of PEG-HCA1 Im at several temperatures.

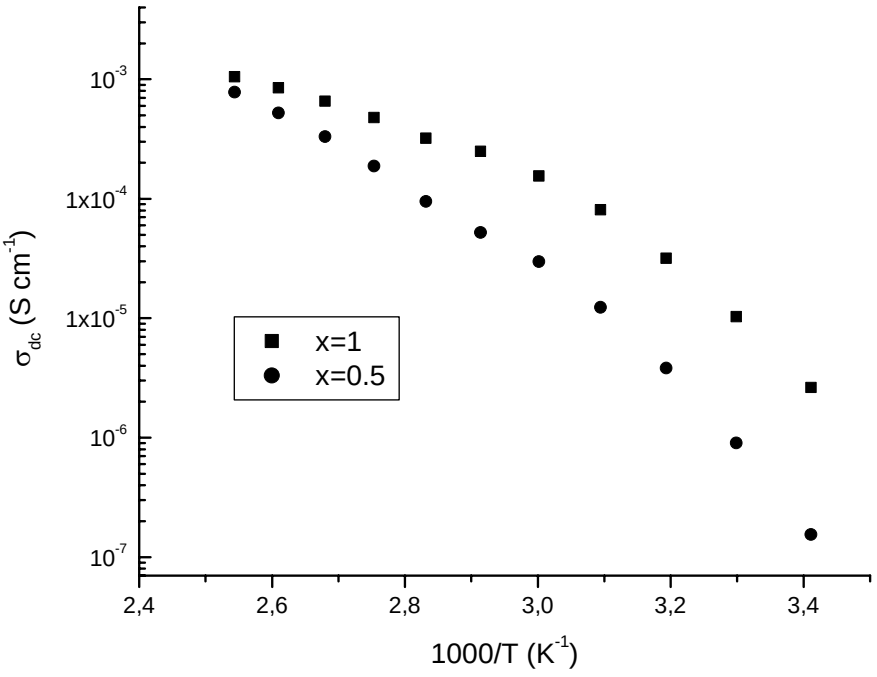

Figure 6.18 Temperature dependence of DC conductivities, PEG-HCAxIm.

6.5.5 Proton Conductivities of The Homopolymer and Composites

Proton conductivities of the PEGMAP, Poly(PEGMAP-$Im_{0.75}$), Poly(PEGMAP-Im_1) and Poly(PEGMAP-$BnIm_1$) were determined via ac impedance technique over the frequency range 1 Hz to 1 MHz at various temperatures. The PEGMAP and composites are insoluble and hence has no good film-forming properties. The pellets of the materials were sandwiched between gold-coated electrodes and their conductivities were measured under dry-nitrogen atmosphere.

The temperature and frequency dependence of alternating current, AC conductivities of homopolymer and composites displayed in Figures 6.19, 6.20, 6.21 and 6.22. The proton conductivity was obtained by repeating heating/cooling measurements on the same sample, from 0 to 160 ^{o}C. σ_{ac} versus frequency curves consist of the frequency independent conductivity plateau regions, which are well developed at low frequencies and at low temperatures shifts toward higher frequencies with increasing temperature.

The DC conductivity (σ_{dc}) of the samples was derived from the plateaus of log σ_{ac} vs. log F by linear fitting the data. The σ_{dc} values obtained by this method coincide well with the one that acquired from Z' minimum in the real and imaginary ratio (Z'/Z") plot of impedance, so that taking the values extrapolated from σ_{ac} plateaus to be good estimation. At higher temperatures (T > 60 ^{o}C) and in the low frequency zone, the fall in the conductivity is due to polarization of the blocking electrodes.

The anhydrous proton conductivities of PEGMAP, Poly(EGMAP- $Im_{0.75}$), Poly(EGMAP-m_1) and Poly(EGMAP-$BnIm_1$) are illustrated in 6.23, 6.24, 6.25 and 6.26. In order to enhance the defect type proton conductivity, heterocyclic units were intercalated into the host polymer. The anhydrous conductivity of PEGMAP-Im or BnIm increased with mixing ratio and the temperature. A marked curvature in the conductivity isotherms is observed for all the composite electrolytes that can be interpreted with the Vogel-Tamman-Fulcher (VTF) equation (Eq. 6.23). The contribution of segmental relaxation to the conductivity is verified by inserting the VTF fits into Figure 6.5 (dash lines). The fit parameters are compiled in Table 6.2. Imidazole and benzimidazole which are heterocyclic organic molecules, conducts protons via structure diffusion (Grotthuss Mechanism), i.e., intermolecular proton jump and reorientation within a hydrogen bonded network (Kreuer et al., 1998). It was reported that pKa for imidazole is approximately 14.9 while the pKa for imidazolium is about 7 for benzimidazole the corresponding pKa values are 12.9 and 5.3 (Münch et al., 2001). Intercalation of imidazole or benzimidazole into PEGMAP results in the formation of protonated and unprotonated heterocycles. An electrostatic interaction forms between –P-O^{-} anions and imidazolium or benzimidazolium ions. Partial deprotonation of phosphonic acid and protonation of heterocyclic units are proved by FT-IR spectra of the composite electrolytes. These phenomena imply that the defect type conduction occurs through intermolecular proton exchange reactions between neighboring heterocyclic molecules. Since molecular structure of Im that constructs molecular cluster, including approximately 20 molecules through hydrogen bonding (Münch et al., 2001).

Correspondingly, maximum proton conductivity of Poly(EGMAP-Im_1) and Poly(EGMAP-BIm_1) was found to be 2 x 10^{-4} S/cm and 3.5 x 10^{-5} S/cm at 160 ^{o}C in the anhydrous state. The higher activation energy and lower conductivity at lower

temperatures of the Poly(EGMAP-BIm$_1$) system indicates a lower local proton mobility due to molecular structure of benzimidazole.

Table 6.2 Maximum Anhydrous Proton Conductivities and VTF Parameters (T_o and B) for the Polymer/Heterocycle Composite Electrolytes.

Composite Electrolytes	Max. Conduct. (S/cm) at 160 ^oC	T_o (K)	B (eV)
Poly(PEGMAP-Im$_1$)	$2x10^{-4}$	202	0.22
Poly(PEGMAP-Im$_{0.75}$)	$5.2x10^{-5}$	211	0.19
Poly(PEGMAP-BnIm$_1$)	$3.8\ x10^{-5}$	225	0.26

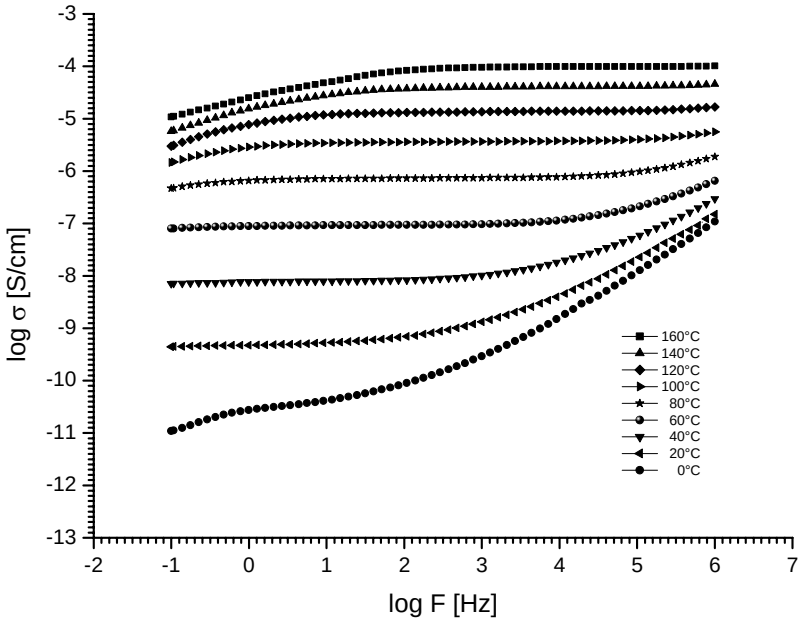

Figure 6.19 AC conductivity of PEGMAP at several temperatures.

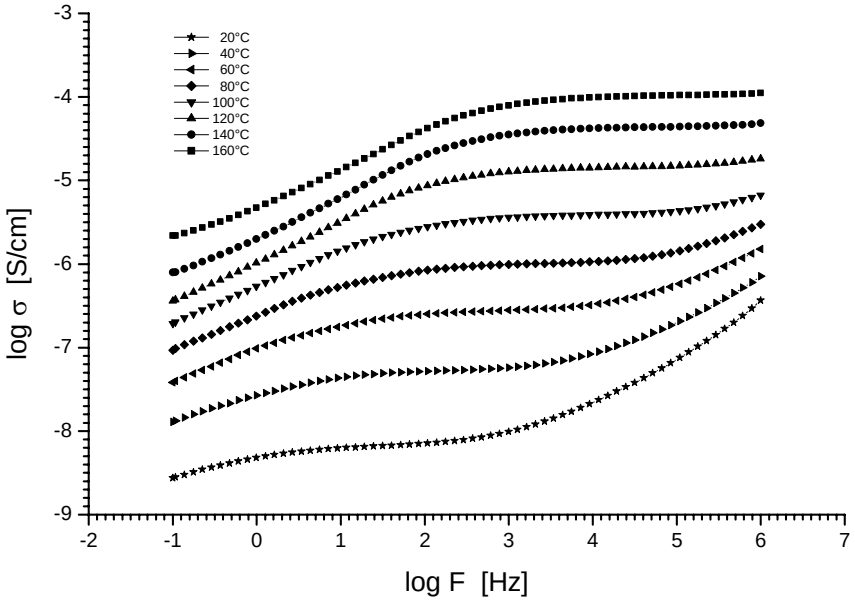

Figure 6.20 AC conductivity of PEGMAP 0,75 Im at several temperatures.

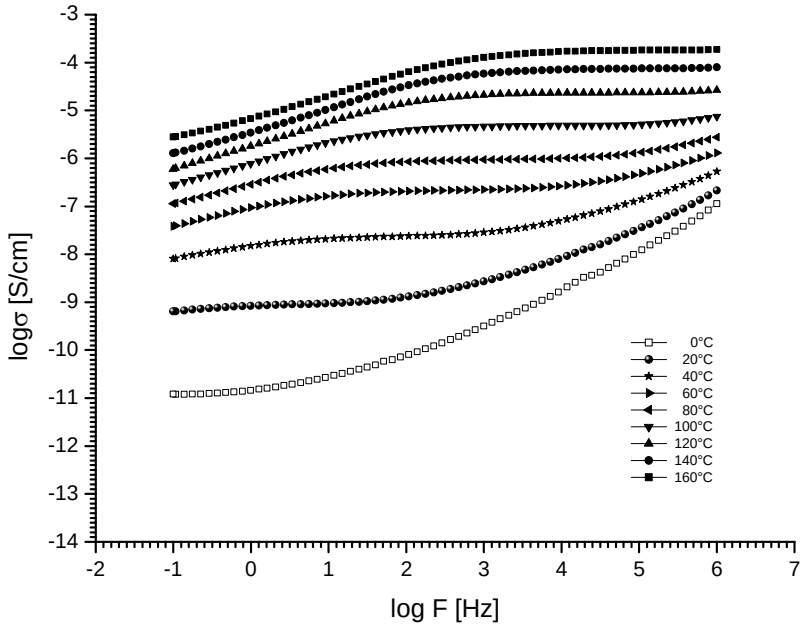

Figure 6.21 AC conductivity of PEGMAP 1 Im at several temperatures.

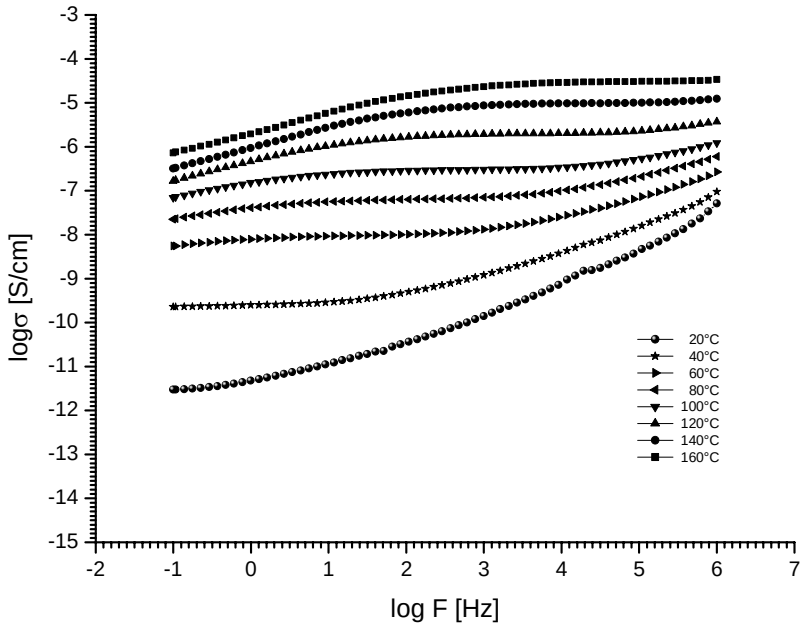

Figure 6.22 AC conductivity of PEGMAP 1 BnIm at several temperatures.

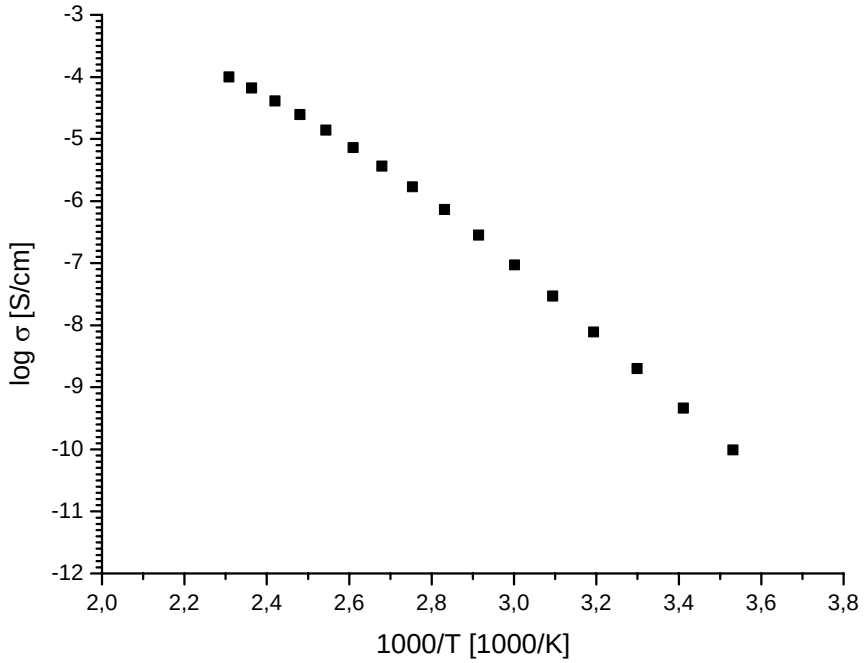

Figure 6.23 Temperature dependence of DC conductivities, PEGMAP.

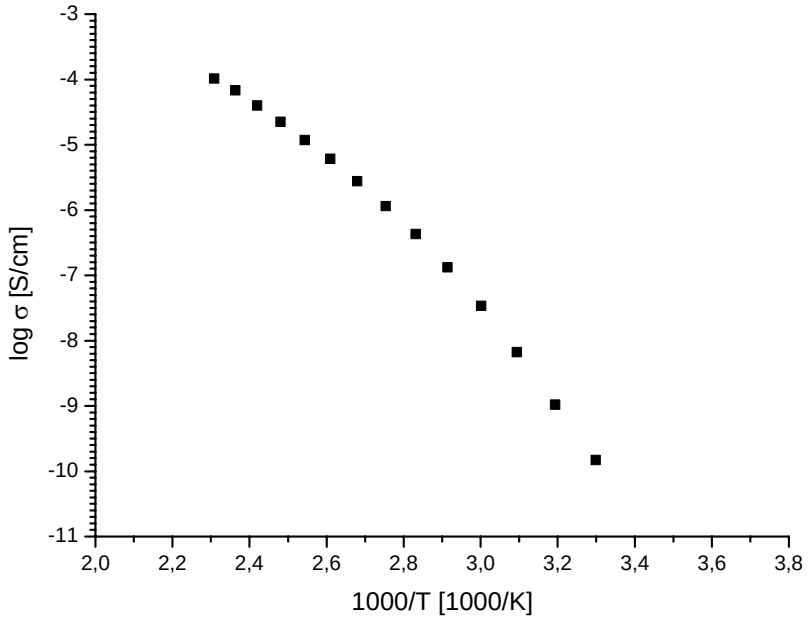

Figure 6.24 Temperature dependence of DC conductivities, PEGMAP 0,75 Im.

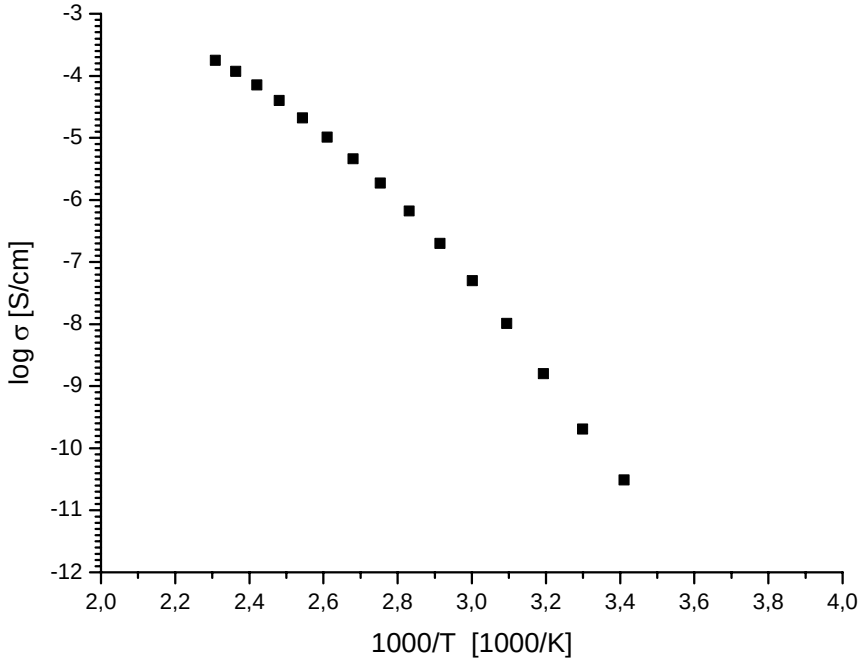

Figure 6.25 Temperature dependence of DC conductivities, PEGMAP 1 Im.

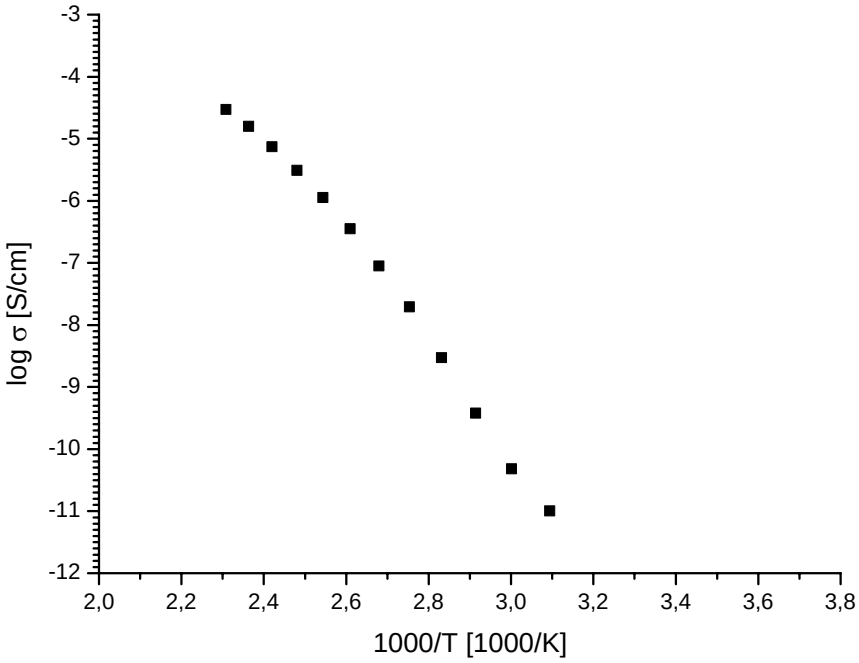

Figure 6.26 Temperature dependence of DC conductivities, PEGMAP 1 BnIm.

CHAPTER 7

CONCLUSION

In this study, novel anhydrous proton conducting electrolytes were prepared by means two different approaches.

In the first, polyethylene glycol carboxylate, PEG-HCA was doped with imidazole (Im) at various stoichiometric ratios to form PEGCAxIm where x is the molar ratio of Im to –COOH unit. The FT-IR study indicate by the transfer of the acidic proton of the carboxylic acid to the ‘‘free’’ nitrogen side of imidazole to form imidazoliumion. PEGCAxIm complexes the initial weight reduction starts at 182 ^{o}C both x = 0.5 and x = 1. The Tg of the blend is -4^{o}C for x=0.5 and x=1 -22^{o}C for x = 1. The blends of the PEGCA1Im exhibited a maximum proton conductivity of approximately 10^{-3} S/cm at 120 ^{o}C.

In the second, novel anhydrous proton conducting polymer-heterocyle composite electrolytes were investigated. The The Poly(EGMAP-Im_x) or Poly(EGMAP-$BnIm_x$) materials were produced by free-radical bulk polymerization of ethylene glycol methacrylate phosphate in the presence of proton solvents such as imidazole or benzimidazole. The composite electrolytes were insoluble in organic solvents and almost no dopant loss was observed when the materials were placed in THF or methanol. The thermal and conductivity properties of homopolymer are improved by intercalation of heterocyclic units. Temperature dependence of proton conductivity follows VTF behavior which suggests the contribution of segmental relaxation to structure diffusion. Poly(EGMAP-Im_1) showed a conductivity of 2 x 10^{-4} S/cm at 160 ^{o}C. The utilization of bulk polymerization method is rather new and cheap for composite electrolyte synthesis.

REFERENCES

Acheson, R.M., "An introduction to the chemistry of heterocyclic compounds", 3rd ed. Canada, Wiley, 1976.

Allcock, H.R., Hofmann, M.A., Ambler, C.M., "Phenyl phosphonic acid functionalized polywaryloxyphosphazenesx as proton-conducting membranes for direct methanol fuel Cells", *Journal of Membrane Science*, Vol. 201, pp. 47 –54, 2002.

Armand, M., "Polymer solid electrolytes-An Overview ", *Solid State Ionics*, Vol. 9&10, pp.745-754, 1983.

Asensio, J.A., Borro´s, S., Go´mez Romero, "Proton conducting polymers based on benzimidazole and sulfonated benzimidazoles", *Journal of Polymer science: PolymChem*. Vol. 40, pp. 3703 –10, 2002.

Bae, J.M., Honma, I., Murata, M., Yamamoto, T., Rikukawa, M., Ogata, N., "Properties of selected sulfonated polymers as proton-conducting electrolytes for polymer electrolyte fuel cells", *Solid State Ionics*, Vol. 147, pp. 189 –94, 2002.

Berzins, T., *Journal of Electrochemical Society*, Vol. 124(8), pp. C318, 1977.

Besse, S., Capron, P., Diat, O., "Sulfonated polyimides for fuel cell electrode membrane assemblies (EMA)", *Journal of New Material Electrochemical Systems*, Vol. 5, pp. 109 –12, 2002.

Bloys van Treslong, C.J., Staverman, A.J., *Rec. Trav. Chim., Pay-Bas*, Vol. 93(6) , pp. 171– 78, 1974.

Blythe, A.R., *Electrical Properties of Polymers*, Cambridge University Pres, pp.38-71 Cambridge, 1979.

Bozkurt, A., Meyer, W.H., Wegner, G., "PAA/imidazol-based proton conducting polymer electrolytes", *Journal of Power Sources*, Vol. 123, pp.126–131, 2003.

Bozkurt, A., Meyer, W.H., *Journal of Polymer science: Polymer Physics*, Vol. 39, pp. 1987, 2001.

Bozkurt, A., Meyer, W.H., Wegner, G., *Journal of Power Sources*, Vol. 123, pp. 126, 2003.

Bozkurt, A., *Turkish Journal of Chemistry*, Vol. 29, pp. 117, 2005.

Bozkurt, A., Meyer, W.H., *Solid State Ionics* , Vol. 138, pp. 259–265, 2001.

Brennan, W.P., *Thermochimica Acta,* Vol. 18 pp.101-111, 1977.

Buckley, A., Stuetz, D.E., Serad, G.A., *In Encyclopedia of Polymer Science and Engineering*, Second Edition, Vol. 11, pp.572–601, New York, Wiley & Sons, 1988.

Carter, R., Wycisk, R., Yoo, H., Pintauro, P.N., *Electrochemica Solid State Letter*, Vol. 5, pp. A195 – A197, 2002.

Chen, R., Yang, R., Durand, B., Pradel, A., Ribes, M., *Solid State Ionics*, Vol. 53-56, pp.1194-1199, 1992.

Chen, S.L., Krishnan, L., Srinivasan, S., Benziger, J., Bocarsly, A.B., *Journal of Membrane Science*, Vol. 243, pp. 327, 2004.

Chin, D.T., Chang, H H., *Journal of Applied Electrochemistry,* Vol. 19(1), pp. 95–99, 1989.

Chowdari, B.V.R., Gopalakrishnan, R., *Solid State Ionics,* Vol. 23, pp.225-233, 1987.

Cowie, J.M.G., Sadaghianizadeh, K., *Solid State Ionics,* Vol. 42, pp.243, 1990.

Compbell, I.M., "Introduction to Synthetic Polymers", Oxford University Press, 1994.

Compell, D., White,J.R., " Polymer Characterization", Chapman & Hall, NJ 1989.

Craver, C.D., "Polymer Characterization" , Ch.12, American Chemical Society, 1983.

Crompton, T.R., "Analysis of Polymers", Pergamon Pres, pp. 16, 1989.

Daniel, M.F., Desbat, B., Cruege, F., Trinquet, O., Lass`egues, J.C., *Solid State Ionics* , Vol. 28, pp. 637–41, 1988.

DesMarteau, D. D., *Journal of Fluorine Chem.,* Vol. 72, pp. 203 ~1995!.

Ding, J., Chuy, C., Holdcroft, S., *Adv Funct Mater* ., Vol. 12, pp. 389 –94, 2002.

Dippel, T., Kreuer, K.D., Lass`egues, J.C., Rodriguez, D., *Solid State Ionics,* Vol. 61(1–3), pp. 41–46, 1993.

Dominiquez , L., Meyer, W.H., *Solid State Ionics,* Vol. 28-30, pp.941-949, 1988.

Donoso P, Gorecki W, Berthier C, Defendini F, Poinsignon C, Armand MB. *Solid State Ionics* Vol. 28, pp. 969–74, 1988.

Doyle, M., Wang, L., Yang Z., Choi, S. K., *Journal of Electrochemical Society,* Vol. 150, pp.185, 2003.

Erdemi, H., Bozkurt, A., Meyer, W.H., *Synthetic Metals*, Vol. 143 pp. 133, 2004.

Fontanella, J.J., Wintersgill, M.C., Wainright, J.S., Savinell, R.F., Litt, M., *Electrochimica Acta,* Vol. 43(10–11), pp.1289–94, 1998.

Genies, C., Mercier, R., Sillion, B., Cornet, N., Gebel, G., Pineri, M., *Polymer* ,Vol. 42 ,pp. 359 –73, 2001.

Genies, C., Mercier, R., Sillion, B., *Polymer* ,Vol. 42, pp. 5097 –105, 2001.

Gillham, J.K., *Macromolecule Science,* Vol. 1, pp.83, 1972.

Glipa, X., Bonnet, B., Mula, B., Jones, D.J., Rozi`ere, J., *Journal of Material Chem.* , Vol. 9(12), pp. 3045–49, 1999.

Grot, W., To E.I. du Pont de Nemours and Company, U.S. 3,718,627, 1968.

Guo, X., Fang, J., Watari, T., Tanaka, K., Kita, H., Okamoto, K., *Macromolecules* Vol. 35, pp. 6707 –13, 2002.

Hickner, M.A., "Transport and Structure in Fuel Cell Proton Exchange Membranes", 2003.

Hofmann, M.A., Ambler, C.M., Maher, A.E., *Macromolecules*, Vol. 35, pp. 6490 –3, 2002.

Hogarth, M., Glipa, X., *High Temperature Membranes For Solid Polymer Fuel Cells*, ETSU F/02/00189/REP DTI/Pub URN 01/893 ~2001.

Hogdon, R. B., *Jornal of Polymer Science,: Gen. Pap.*, Vol. 6, pp. 171, 1968.

Jang, L.K., Nguyen, D., Geesey, G.G., Water Res Vol. 33, pp. 2826, 1999.

Jannasch, P., *Current Opinion in Colloid and Interface Science*, Vol. 8, pp. 96, 2003.

Jo¨nissen, L., Gogel, V., Keres, J., Garche, J., *Journal of Power Sources,* Vol. 105, pp. 267 –73, 2002.

Karadedeli, B., Bozkurt, A., Baykal, A., Physica, Vol. B 364, pp. 279–284, 2005.

Kim, J.D., Honma, I., *Solid State Ionics* ,Vol. 176 pp. 979-984, 2005.

Kreuer, K.D., *Solid State Ionics,* Vol. 136– 137, pp. 149–60, 2000.

Kreuer, K.D., Fuchs, A., Ise, M., Spaeth, M., Maier, J., *Electrochimica Acta*, Vol. 43, pp.1281–1288, 1998.

K.D. Kreuer., Proceedings of the sixth Asian Conference on Solid State Ionic : Science and Technology, 29 Novamber-4 December, pp.263, New Delhi, 1998.

Kreuer K.D., Dipel, Th., Meyer. Wh., Maier, J., "Perfluorinated Ionemer Membranes", *Proceedings of the First International Symposium on Material Research Society*, 10-21 April, Vol. 293, pp. 273-282, Mainz, 1998.

Kreuer, K.D., *Journal of Membrane Science*, Vol. 185, pp. 29 –39, 2001

Kotov, S.V., Pederesen, S.D., Qui, W. Z.-M ., Burton, D. J., *Jornal of Fluorine Chem.*, Vol. 82,pp. 13 ~1997.

Kreuer, K.D., *Chemistry Materials*, Vol. 8, pp.610–641, 1996.

Kawahara, M., Rikukawa, M., Sanui, K., Ogata, N., *Solid State Ionics* , Vol. 136– 137, pp. 1193 –6, 2000.

Kawahara, M., Rikukawa, M., Sanui, K., *Polymer Advanced Technology* , Vol. 11, pp. 544 –7, 2000.

Laskar, A.L., Chandra, S., "Superionic Solids Electrolytes Recent Trends", Academic Press, Inc., 1989.

Lass`egues, L.C., Desbat, B., Trinquet, O., Cruege, F., Poisignon, C., *Solid State Ionics*, Vol. 35(1–2), pp. 17–25, 1989.

Li, M., Hibino, M., Miyayama, M., Kudo, T., *Solid State Ionics*, Vol. 134, pp. 271, 2000.

Li, Q., Hjuler, H.A., Bjerrum, N.J., *Journal of Applied Electrochemistry*, Vol. 31(7), pp.773–79, 2001.

Lide DR,. Handbook of Chemistry and Physics. Boca Raton: CRC Press. 76th ed. 1995.

Linford, R.G., *Electrochemical Science and Technology of polymers*, Ch. 7, Elsevier Science Publishers LTD., 1990.

Liu, W., Ruth, K., Rusch, G., *Journal of New Material Electrochemical Systems*, Vol. 4, pp. 227, 2001.

Munson, R.A., *Journal of Physical Chemistry*, Vol. 68(11), pp. 3374–77, 1964.

Munson, R.A., Lazarus, M.E., *Journal of Physical Chemistry* , Vol. 71(10), pp. 3245–48, 1967.

Münch, W., Kreuer, K.D., Silvestri, W., Maier, J., Seifert, G., *Solid State Ionics* , Vol. 145, pp. 437–443, 2001.

Qingfeng, L., Hjuler H.A., Bjerrum,N.J., *Journal of Applied Electrochemistry*, Vol. 31, pp.773 –9, 2001.

Rodriguez, D., Jegat, C., Trinquet, O., Grondin, J., Lass`egues, J.C., *Solid State Ionics*, Vol.61(1–3), pp. 193–202, 1993.

Poppe, D., Frey, H., Kreuer, K.D., Heinzel, A., Mu¨lhaupt, R., *Macromolecules*, Vol. 35, pp. 7936 –41, 2002.

Pourcelly, G., Oikonomou, A., Hurwitz, H.D., Gavach, C., *Journal of Electroanalytical Chemistry*, Vol. 287, pp. 43-59, 1990.

Przyluski, J., Wieczorek, W., *Synthetic Metals*, Vol. 45, pp. 323-333, 1991.

Pu, H., Meyer, W.H, Wegner, G., *Journal of Polymer science: Polymer Physics*, Vol. 40(7), pp. 663– 69, 2002.

Ratner, *Polymer Electrolyte Reviews*, Maccllum, J.R., and C.A. Vincent (editors), Ch. 7, Applied Science Publihers L.T.D., 1987.

Reisinger, T.J.G., "Abhängigkeit der Leitfähigkeit Glasartiger Ionene von Druck und Temperatur" , Ph. D. Thesis, Johannes Gutenberg- Universitt, 1998.

Rieke, P.C., Vanderborgh, N.E., *Journal of Membrane Science*, Vol. 32, pp. 313-328, 1987.

Rietz, R.R., Rohr, K.S., Meyer, W.H., Spiss, H.W., Wegner, G., *Solid State Ionics*, Vol. 68, pp.151-158, 1994.

Rikukawa, M., Inagaki, D., Kaneko, K., Takeoka, Y., Ito, I., Kanzaki, Y., Sanui, K., *Journal of Molecular Structure*, Vol. 739, pp. 153, 2005.

Samms, S.R., Wasmus, S., Savinell, R.F., *Journal of Electrochemical Society*, Vol. 143, pp.1498,1996.

Savett, S. C., Atkins, J. R., Sides, C. R., . Harris, J. L., . Thomas, B.H., Creager, S. E., Pennington, W.T., DesMarteau, D. D. , *Journal of Electrochemical Society*, Vol. 149, pp. A1527, 2002.

Savadogo, O., Varela, F.J.R., *Journal of New Material Electrochemical Systems* , Vol. 4(2), pp.93–97, 2001.

Sevil, F., Bozkurt, A., *Journal of Physics and Chemistry of Solids*, Vol. 65(10) pp. 1659, 2004.

Sevil, F., Bozkurt, A., *Turkish Journal of Chemistry*, Vol. 29, pp. 117, 2005.

Schuster M.F.H., Meyer W.H.., *AnnualReviewofMaterials Research*, Vol. 33, pp. 233-261, 2003.

Schechter A., Savinell, R.F., *Solid State Ionics*, Vol. 147, pp.181, 2002.

Schoolman, D., Trinquet, O., Lass`egues, J.C., *Electrochimica Acta*, Vol. 37(9) , pp.1619–21, 1992.

Schuster M.F.H., Meyer W.H.., Kreuer K.D., *Chemical Materials*, Submitted.

Schuster, M., Meyer, W.H., Wegner, G., *Solid State Ionics*, Vol. 145, pp. 85 –92, 2001.

Singleton, R.W., Noether, H.D. ,Tracy, J.F., *Journal of Polymer Science: Polymer Symposium* , Vol. 19, pp.65–76, 1967.

Smitha, B., Sridhar, S., Khan, A.A., *Journal of Membrane Science*, Vol. 259, pp. 10, 2005.

Steck A. E., Stone, C., in *Proceedings of the 2nd International Symposium on New Materials for Fuel Cell and Modern Battery Systems*, O. Savagodo, P. R. Roberge, and T. N. Veziroglu, Editors, Montreal, Quebec, Canada, July 6-10, 1997, 792 ~1997.

Sumner, J.J., Creager, S.E., Ma, J.J.A., DesMarteau, D.D., *Journal of Electrochemical Society*, Vol. 145, pp.107,1998.

Sun, R.J., Jordan, L., Forsyth, M., MacFarlane, D., *Electrochimica Acta*, Vol. 46, pp. 1703, 2001.

Takahashi, T., "High Conductivity Solid Ionic Conductors", World Scientific Publications Co. Ptc. Ltd..,1989.

Tanaka, R., Yamamoto, H., Kawamura, S., Iwase, T., *Electrochimica Acta* ,Vol. 40(13) , pp. 2421–29, 1995.

Tanaka, R., Yamamoto, H., Shono, A., Kubo, K., Sakurai, M., *Electrochimica Acta*, Vol. 45 (8–9) , pp. 1385–89, 2000.

Tang, H., Pintauro, P.N., *Journal of Applied Polymer Science*, Vol. 79, pp. 49 –59, 2001.

Wainright, J.S., Wang, J.T., Weng, D., Savinell, R.F., Litt, M., *Journal of Electrochemical Society* , Vol. 142(7), pp. L121–23, 1995.

Wainright, J.S., Wang, J.T., Savinell, R.F., Litt, M., Moaddel, H., Rogers, C., "In Electrode

Materials and Processes for Energy Conversion and Storage", Proceedings of the Symposium on Electrode Materials and Processes for Energy Conversion and Storage II, Srinivasan, S.,

Macdonald, D.D., Khandkar, A.C.,(editors), PV 94-23, p. 255, The Electrochemical Society. Proceedings Series, Pennington, NJ, 1995.

Wang, F., Hickner, M., Kim, Y.S., Zawodzinski, T.A., McGrath, J.E., *Journal of Membrane Science* , Vol. 197, pp. 231 –42, 2002.

Wasmus, S., Daunch, A., Moaddel, H., Rinaldi, P.L., Litt, M., Presented at 187 th *Electrochem. Soc.* Meet. Reno. Abstr. 466, 1995.

Wundelich, B., "Thermal Analysis", Ch.7, Academic pres, Inc., 1990.

Yamada, M., Honma, I., *Journal of Physical Chemistry*, Vol. 108, pp. 5522, 2004.

Yamada, M., Honma, I., *Electrochimica Acta*, Vol. 48, pp. 2411, 2003.

Yamada, M., Honma, I., Chem Phys. Chem. Vol. 5, pp. 724, 2004.

Yamada, M., Honma, I., *Polymer* , Vol. 45, pp. 8349-8354, 2004.

Yamada, M., Honma, I., Angew Chem, Int Ed., Vol. 43, pp. 3688, 2004.

Yamada, M., Honma, I., *Electrochimica Acta* , Vol. 50, pp. 2837–2841, 2005.

Yamada, M., Honma, I., *Polymer*, Vol. 46, pp.2986, 2005.

Yeo, R.S., McBreen, J.C., *Journal of Electrochemical Society*, Vol. 130, pp.533, 1983.